

**FACULTY
OF MATHEMATICS
AND PHYSICS**
Charles University

MASTER THESIS

Sára Belejová

**Cellular protein interactions studied by
advanced fluorescence imaging methods**

Institute of Physics

Supervisor of the master thesis: prof. RNDr. Petr Heřman, CSc.

Study programme: Biophysics and Chemical Physics

Study branch: Experimental biophysics and
chemical physics

Prague 2023

I declare that I carried out this master thesis independently, and only with the cited sources, literature and other professional sources. It has not been used to obtain another or the same degree.

I understand that my work relates to the rights and obligations under the Act No. 121/2000 Sb., the Copyright Act, as amended, in particular the fact that the Charles University has the right to conclude a license agreement on the use of this work as a school work pursuant to Section 60 subsection 1 of the Copyright Act.

In date

Author's signature

I want to thank my supervisor prof. RNDr. Petr Heřman, CSc. for his guidance, patience, advice, and positivity. Thanks also belongs to my consultant Mgr. Dita Strachotová, Ph.D. for her time, willingness to help, and diligent writing of notes that have always kept us on track. For preparing all the samples used in this work, his sincere interest, and a great laboratory excursion, I thank my second consultant, Aleš Holoubek, Ph.D.

I would also like to thank my friends who endured the hardships of studying with me and supported me verbally or with a piece of chocolate and a glass of wine whenever needed.

Many thanks to my wonderful family who always believed in me but never put pressure on me.

Finally, I want to thank my fiancé Jakub who taught me not to give up easily and always sees more in me than I do in myself.

Title: Cellular protein interactions studied by advanced fluorescence imaging methods

Author: Sára Belejová

Institute: Institute of Physics

Supervisor: prof. RNDr. Petr Heřman, CSc., Institute of Physics

Abstract:

This thesis studies an important tumor suppressor, p53, and its interaction partner, nucleophosmin (NPM), in living cells. Proteins are studied using fluorescence confocal microscopy techniques such as fluorescence lifetime imaging and fluorescence anisotropy measurements. The primary focus of the research is on a specific variant of the p53 protein called p53-L344P, which is generated by a point mutation from its original form (p53wt). We investigate the oligomerization state of p53-L344P *in vivo*, which appears to be monomeric, confirming the results of *in vitro* experiments from other studies. Further, we show that p53wt and p53-L344P can form complexes with each other. We compare the interaction of the NPMmutA protein with p53wt and p53-L344P proteins. Our findings reveal that the L344P mutant is not transferred from the nucleus to the cytoplasm in the presence of NPMmut, as is p53wt. Furthermore, we investigate the oligomerization state of p53wt when it is in the cytoplasm and propose avenues for further research into this interaction.

Keywords: confocal microscopy, time-resolved fluorescence, FLIM, FRET, homoFRET, fluorescence anisotropy, fluorescence proteins, protein interactions

Contents

Introduction	3
1 Nuclear proteins	5
1.1 p53 protein	5
1.2 Nucleophosmin	6
2 Fluorescence microscopy	9
2.1 FRET and homoFRET	11
2.2 FLIM and TCSPC	12
2.3 Anisotropy imaging	12
2.4 Fluorescent proteins	14
3 Samples and methods	15
3.1 Sample preparation	15
3.1.1 Cell cultivation and plasmid transfections	15
3.1.2 Plasmid construction	15
3.2 Microscopy - technical equipment	15
3.3 Measurement calibration	16
3.4 Data acquisition and processing	18
3.4.1 HeteroFRET experiments (FLIM measurement)	18
3.4.2 HomoFRET experiments (steady-state and time resolved anisotropy measurement)	19
4 Results	22
4.1 p53 variants	22
4.1.1 p53wt	22
4.1.2 p53mut	23
4.1.3 mRFP1 labeled p53 constructs	26
4.1.4 p53wt and p53mut interactions	28
4.2 NPMcut	28
4.3 NPM and p53 variants	30
4.3.1 NPMmut and p53wt	31
4.3.2 NPMmut and p53mut	35
4.3.3 NPMmutcut and p53	36
4.3.4 NPMmutcut and p53wt	36
4.3.5 NPMmutcut and p53mut	36
5 Discussion	39
5.1 Discussion of the results	39
5.2 Asymmetry of reverse fluorescent labeling	42
5.3 Time-resolved anisotropy analysis	43
Conclusion	44
Bibliography	45

List of Figures	49
List of Tables	50
A Review of anisotropy decay fitting	51

Introduction

Luminescence - the excess of light emission over thermal radiation (cold light) with a finite duration is a fascinating phenomenon that has naturally interested people since ancient times [1, 2]. Today we know that it is the emission of light from the excited state of the substance, and we can categorize it according to the source of excitation (photoluminescence, chemiluminescence, triboluminescence, bioluminescence, etc.). Photoluminescence, which includes fluorescence and phosphorescence, has naturally become the subject of research, and even though its process was clarified only in the last 150 years, today, its principle is used by a considerable number of imaging techniques [3, 4]. Thanks to the development of lasers and beam scanning, sensitive detectors and cameras, and data-analyzing software, some fluorescence techniques were developed even beyond the resolution of the diffraction limit [5].

Since the discovery of fluorescent proteins, used as fluorescent markers and probes, fluorescence microscopy is, thanks to genetic engineering [6], used in almost every biological discipline, from microbiology to systems physiology. These unique probes have proven extremely useful in tracking the localization and dynamics of proteins, organelles, and other cellular compartments, providing a window to cellular structure and function *in vivo* [7, 8, 9, 10].

In living organisms, there is a tight connection between the localization, structure, and functionality of proteins [11, 12]. Therefore, it is beneficial to investigate these properties in the context of the cell. To this end, our laboratory employs fluorescence lifetime imaging microscopy and fluorescence anisotropy measurements described in the theoretical introduction.

In cooperation with the Institute of Hematology and Blood Transfusion, our department studies proteins related to cancer diseases. The latest research has focused on the interaction between the nuclear proteins p53 and nucleophosmin (NPM) [13], finding that NPM mutated typically for AML (NPMmut) and NPMmut variant with truncated oligomerization domain, interacts with p53 and pulls the p53 protein out of the nucleus into the cytoplasm. As exclusive cytoplasmic localization of p53 is not conducive to its proper cellular function, it is crucial to investigate the mechanisms behind this delocalization and explore strategies to restore p53's nuclear localization.

In this work, we want to examine the influence of the oligomeric state of the p53 protein on its interaction with NPM. Therefore, we will investigate the mutated form of the p53 protein created by a point mutation - L344P, which, according to the literature, should exist in the cell in a purely monomeric state [14].

Exploring this specific mutation is of particular significance as it is also found in patients with Li-Fraumeni syndrome [15]. Li-Fraumeni syndrome [16] is a rare hereditary condition associated with an increased risk of developing various cancers (especially in the early stages of life) due to a mutation in the gene encoding the p53 protein. These are especially sarcomas (cancers of muscle, bone, or connective tissue), breast cancer, and adrenocortical cancer [17].

Since the fluorescence anisotropy method that we use to investigate the oligomerization state of proteins is still under development in our laboratory, measure-

ments with the mutated variant of p53 will be compared with its wild-type form to validate the method. As controls, we will also employ oligomerizing NPM-mut and a non-oligomerizing variant of NPM obtained by cutting the N-terminal oligomerization domain labeled with fluorescent proteins.

In terms of content, this thesis provides an introduction to the proteins under study, explores the basic principles of fluorescence and associated processes, discusses experimental techniques, including sample preparation, equipment, measurement procedures, and data analysis, presents the results obtained, engages in thorough discussions of these findings, and concludes with a comprehensive summary of the research.

1. Nuclear proteins

This chapter aims to provide basic information about a model system of nucleoproteins studied in this thesis.

1.1 p53 protein

p53 is a nuclear protein of the size of 53 kD, coded by TP53 gene [18]. It is an important tumor suppressor with a key role in response to cellular stress. When activated, p53 transcriptionally regulates multiple biological processes, including DNA damage repair, cell cycle arrest, apoptosis, and senescence. Therefore there is no surprise that its mutation is present in more than 50 % of cancer cases [19], and it is a subject of many studies.

p53 is regulated in the cell by many interaction partners and post-translational modifications [20]. One of the many regulatory pathways includes the MDM2 protein that is bound to p53 at physiological conditions. MDM2 eventually causes ubiquitination and targets p53 for proteasomal degradation. MDM2 might be repressed, among others, by ARF protein. However, when bound with the nucleophosmin ARF is found in the nucleolus, preventing p53 activation [21].

DNA damage promotes a redistribution of ARF to the nucleoplasm, thus promoting p53 activation. NPM protein can also bind directly to MDM2 after nucleoplasmatic redistribution and act as another negative regulator of p53-MDM2 interaction [22]. Activated p53 might cause a cell cycle arrest at the G1/S regulation point by acting on the gene that produces an inhibitor of cyclin-dependent kinases [23]. If DNA is not repaired during the cell cycle arrest, p53 might induce apoptosis.

p53 consists of six main domains: two N-terminal transactivation domains (TADs), a proline rich-domain (PRD), a central DNA-binding domain (DBD), a nuclear localization signal domain (NLS), a tetramerization domain (TD), and C-terminal regulatory domain (CTD) - see Fig.1.1.



Figure 1.1: p53 domain structure. TAD represents the N-terminal transactivation domain, Pro-Rich represents the proline-rich domain, DBD stands for DNA binding domain, NLS stands for the nuclear localization signal domain, TD is the tetramerization domain (NES represents the nuclear export signal and is part of the TD), and C-Reg C-terminal regulatory domain. Adapted from [24].

For the purpose of this work, we were interested in the oligomerization state of the p53 protein. The work of Gaglia [14] showed that at rest, the p53wt protein occurs mainly in dimers, 29 % of the protein exists in unbound monomers, and 13 % forms tetramers. However, after DNA damage, more than 90 % of the protein was bound in tetrameric form.

The importance of the tetrameric form of the protein confirms a number of missense mutations in the TD found in cancer cases. Together with missense mutations in the DBD, it is the most frequent mutation target. The mutation frequency in cancer cases numerically represents $\sim 0.4\%$ per residue in DBD and $\sim 0.66\%$ per residue in TD [24].

Proteins that stabilize or induce tetramerization include MYBBPIA, BCCIP, ArhGAP11A, members of the 14-3-3 family, and some members of a family of calcium-binding proteins known as S100. On the contrary, proteins impeding tetramer form include RBEL1A and ARC (both overexpressed in cancer) and some of the S100 family of calcium-binding proteins [24].

The tetrameric state enables better DNA binding [25, 26] and is responsible for cellular localization, vital for its transcriptional activity. Since nuclear export signal (NES) is part of the TD, tetrameric p53 proteins are typically localized inside the nucleus, while monomeric forms that have NES exposed retain in the cytoplasm. Besides these effects, a non-tetrameric state could cause only partial transcriptional target activation and therefore prefer the outcome of the cell to be solely cell cycle arrest or apoptosis [24].

Many p53 mutant proteins were studied during the past years [27]. One of them is the L344P mutant (Leu at position 344 replaced by Pro - see Fig.1.2). The mutant protein and several others, like L330R/P, R337P, and L342P, were proven to preserve the monomeric form when studied in vitro. The system L344P was chosen to be studied alongside the p53wt protein in this thesis.

From the structural point of view, the tetramerization domain of a p53wt monomer consists of the alfa helix connected with the beta-strand by a tight turn. The p53wt dimer is formed through beta-strands, while two dimers form a tetramer through alfa helices - see Fig.1.3.



Figure 1.2: Tetramerization domain of the p53 wt protein. The figure shows which part of the protein corresponds to the secondary structure of the β -folded sheet and which part corresponds to the α helix. The amino acid highlighted in red (Leucine at position 344) marks where proline is found in the case of the mutated p53 monomeric variant - L344P. Taken and adapted from [24]

1.2 Nucleophosmin

Nucleophosmin (NPM) is a nuclear protein with many functions, including ribosome biogenesis, mRNA processing, chromatin remodeling, embryogenesis, and, last but not least, stabilizing the genome by participating in various DNA repair mechanisms [30]. It is one of the interaction partners of the p53 tumor suppressor.

NPM consists of a hydrophobic core domain at the N-terminal region responsible for oligomerization and chaperone activity [31], followed by an acidic domain required for ribonuclease activity, a basic domain involved in binding nucleic acid,

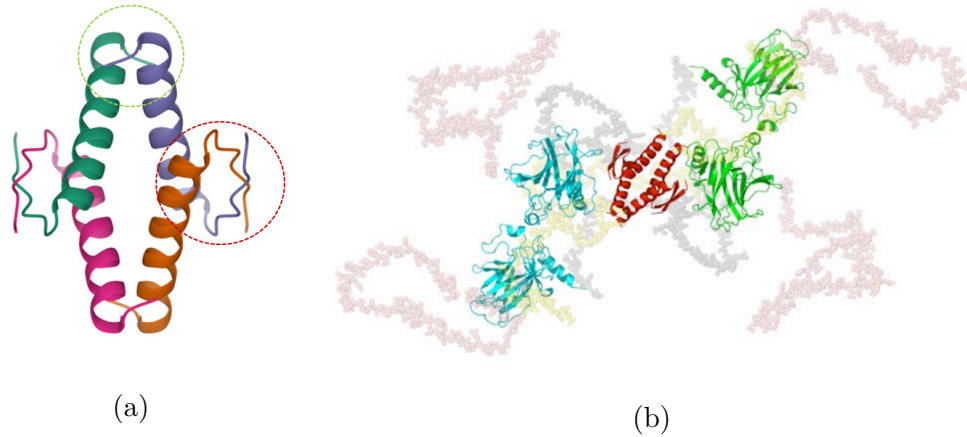


Figure 1.3: flp53 and its tetramerization domain structure. (a) Secondary structure of p53 tetramerization domain. Each color represents the tetramerization domain of a p53 monomer. A red circle marks the monomer-monomer interaction, and a green circle marks the dimer-dimer interaction. The structure is taken from the pdb database, ID: 1AIE [28]. (b) SAXS model of the full-length p53 tetramer (flp53) structure. Core domains (green and cyan) and tetramerization domain (red) are displayed in cartoon representation, while other domains are in a semitransparent spacefill mode. N termini are colored salmon, and C termini are yellow. Taken from [29].

and a C-terminal aromatic stretch required for its nucleolar localization. Crystallization and X-ray diffraction determined the secondary structure of NPM as eight-stranded β -barrel monomers that form a donut-shaped pentamer - Fig. 1.4a [31].

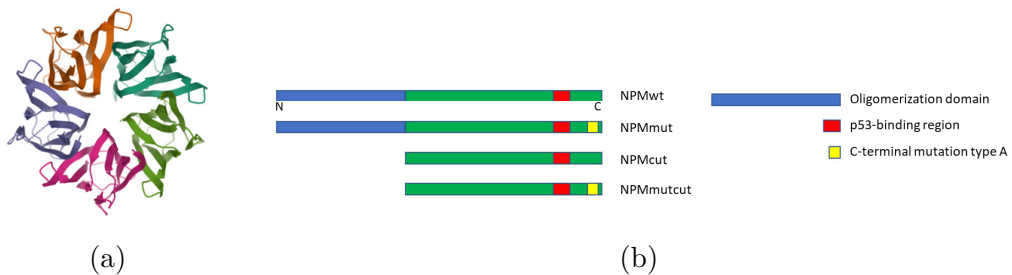


Figure 1.4: (a) Nucleophosmin pentamer structure. (b) Schematic overview of NPM mutations used in the thesis. Taken and adapted from [13].

The cell concentration of the NPM regulates the p53 activation in response to UV radiation [32]. It acts as a natural p53 repressor by preventing premature activation of the p53 defense mechanism [33]; however, it also prevents p53-initiated apoptosis when overexpressed in cancer cells, enabling cancer progression [34].

When talking about NPM in cancer cases, it is usually connected with adult acute myeloid leukemia, where this protein is frequently mutated (about 30 % of cases [35]). The most common mutation, type A, cause the cytosolic localization of NPMmut. Tryptophans W288 and W290 at the C-terminal domain are missing in this mutation [36]. This thesis will study the NPMmut type A and NPM with

cut N-terminal oligomerization domain - NPMcut. NPMcut mutation ensures the monomeric form of NPM protein. Combined mutation, where the oligomerization domain and type A mutation are applied, was also used. The overview of NPM mutation and its markings is shown in Fig.1.4b.

2. Fluorescence microscopy

Fluorescence is a phenomenon that occurs during the transition of an electron between levels with the same multiplicity from an energetically higher level to a lower one (typically from a singlet excited state to a singlet ground state). We can write schematically:



where A^* represents a molecule in the excited state, A represents a molecule in a ground state, h is Planck constant, ν is a wavelength of an emitted photon (together $h\nu$ states for energy emitted from the molecule during fluorescence), and k_f is a rate constant of the process, and it is a function of molecular structure and environment.

It is an emission of electromagnetic radiation (generally visible light) preceded by the absorption of electromagnetic radiation with a shorter wavelength and simultaneous excitation process. Unlike the other type of luminescence, phosphorescence, the transition of an electron between levels with the same multiplicity is a spin-allowed process and therefore happens very quickly, on the order of tens of nanoseconds.

The time for which an electron remains in an excited state before fluorescence occurs is called the fluorescence lifetime. This quantity is the inverse value of the rate constant k_f and serves as a characteristic of fluorophores. Fluorophore lifetime changes when its microenvironment is altered, which is the basis of the imaging technique FLIM (fluorescence lifetime imaging), described in Section 2.2.

Competitive processes to fluorescence are internal conversion, intersystem crossing (both schematically depicted in Fig. 2.1), and energy transfer.

Excitation of a molecule causes rise of electron population on the excited state N . Subsequently these electrons relax to the ground state or its vibrational states. Depopulation of the excited state can be described by the following equation:

$$\frac{dN(t)}{dt} = -k \cdot N(t) \quad (2.2)$$

where t is time and k is rate constant of depopulation. It includes rate constants of radiative and non-radiative transitions: $k = k_r + k_{nr}$. Solution of the equation 2.2 yields:

$$N(t) = N_0 \cdot \exp(-kt). \quad (2.3)$$

where N_0 is the population of excited state at time $t = 0$. Since fluorescence emission intensity is proportional to the number of excited molecules $F(t) \sim N(t)$ we can write:

$$F(t) = F_0 \cdot \exp\left(-\frac{t}{\tau}\right) \quad (2.4)$$

Measuring fluorescent intensity through time means being able to find rate constant k by exponential decay fitting. As mentioned earlier this constant is the inverse of the lifetime τ (an average amount of time a fluorophore remains excited) [4]. Obviously, the more processes causing deexcitation are involved, the faster an exponential decay would be.

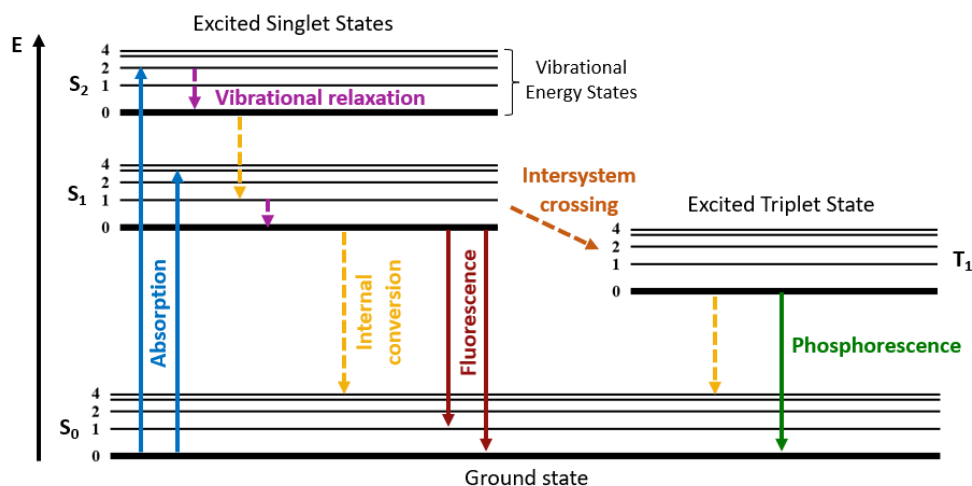
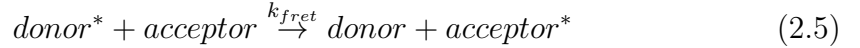


Figure 2.1: Simplified Jablonski diagram; bold line represents electron states, narrow lines represents vibrational states of individual electron states. Straight arrows represent radiative transitions, dashed lines represent non-radiative transitions. At first electron is excited from ground state to the excited states (absorption - blue line) $\sim 10^{-15}$ s. Electrons relax to the lowest vibrational state by vibrational relaxation $\sim 10^{-12} - 10^{-10}$ s and subsequently relax to the ground state by irradiative internal conversion (yellow dashed arrow) $\sim 10^{-11} - 10^{-9}$ s or by radiative process of fluorescence (red line) $\sim 10^{-10} - 10^{-7}$ s. A less probable path for an electron is to change its spin state by intersystem crossing (orange dashed line) $\sim 10^{-10} - 10^{-8}$ s and relax from this state, what is called phosphorescence (green line) $\sim 10^{-6} - 10$ s

2.1 FRET and homoFRET

Förster resonance energy transfer (FRET) is a non-radiative energy transfer caused by dipole-dipole interaction between molecules. One fluorescent molecule acts as an energy donor, while the other as an acceptor. In the process, an excited donor transfers energy to an acceptor, which becomes excited, while the donor deexcites non-radiatively. The acceptor might deexcite radiatively or non-radiatively.



The transfer happens only when the emission spectrum of the donor overlaps with the excitation spectrum of the acceptor, the donor and acceptor are in sufficient proximity, and the molecules have the proper mutual orientation of the donor emission and the acceptor absorption dipole moment.

The distance at which the effectiveness of the FRET is 50 % is described as Förster's distance R_0 and is specific for donor-acceptor pair (ranges in the order of nanometer units).

The rate constant of FRET relaxation mechanism k_{fret} is given in its simplified form as:

$$k_{fret} = \frac{1}{\tau_D} \cdot \left(\frac{R_0}{r_{DA}} \right)^6 \quad (2.6)$$

where τ_D is the emission lifetime of the donor in the absence of the acceptor and r_{DA} is donor-acceptor distance. The lifetime of the donor in the presence of the acceptor is affected as follows:

$$\frac{1}{\tau_{DA}} = k_r + k_{nr} + k_{fret} = \frac{1}{\tau_D} + \frac{1}{\tau_D} \cdot \left(\frac{R_0}{r_{DA}} \right)^6 \quad (2.7)$$

where k_r stands for the rate constant of radiative deexcitation processes and k_{nr} stands for the rate constant of non-radiative deexcitation processes. Altogether $k_r + k_{nr} = k$, which defines the lifetime of the donor in the absence of the acceptor. After rewriting 2.7:

$$\frac{\tau_D}{\tau_{DA}} = k_r + k_{nr} + k_{fret} = 1 + \left(\frac{R_0}{r_{DA}} \right)^6 \quad (2.8)$$

it is evident that the donor's lifetime in the presence of the acceptor is shortened.

We distinguish FRET between two different and two identical molecules, calling the first heteroFRET and the second homoFRET. While in heteroFRET, it is clear which molecule is a donor and which one is an acceptor, in homoFRET situation is different since the role of the donor and the acceptor is interchangeable [37].

As long as the donor and acceptor emit at different wavelengths, it is possible to determine their lifetimes. By photobleaching the acceptor molecule, the FRET mechanism is disabled, and changes in the donor lifetime can be studied.

This is not possible at homoFRET, and different techniques involving emission anisotropy measurements must be applied [4].

2.2 FLIM and TCSPC

Fluorescence lifetime imaging microscopy (FLIM) is an imaging technique that uses the lifetime of present fluorophores as a contrast. The evaluation of the lifetime at each pixel enables to study changes in the fluorophore microenvironment (change in pH, polarity, presence of an analyte).

The technique is usually used in confocal microscopy where out-of-focus fluorescence is rejected, and in multiphoton excitation microscopy, where out-of-plane fluorescence is not excited. In this thesis, a confocal FLIM was used to study changes in lifetime caused by the presence of a heteroFRET acceptor. Due to the sufficient proximity requirement for the efficiency of heteroFRET, it is possible to use this method to investigate protein oligomerization.

Unlike intensity measurements, this technique is not dependent on fluorophore concentrations nor needs a fluorescent acceptor.

To obtain lifetime images, wide-field frequency-domain or laser scanning microscopy methods can be used. Laser scanning microscopy further uses well developed time-correlated single photon counting (TCSPC) method to obtain exponential decay curves.

In TCSPC, a laser pulse excites the molecule and serves as a start signal for time tracking, and the emission photon serves as a stop signal. The time recorded between these two events is stored in a histogram that creates a waveform of the exponential decay of a given fluorophore. Technical details of this method are described in [4].

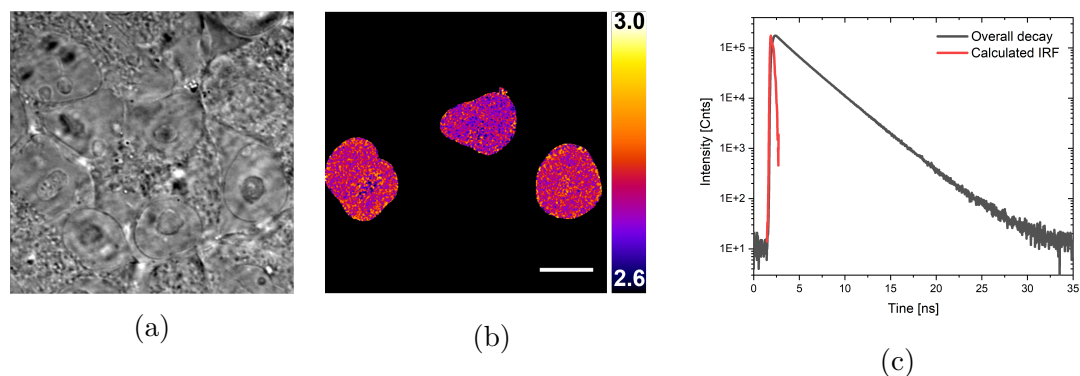


Figure 2.2: (a) Transmission image of cells. (b) Fluorescence lifetime image of cells with p53 protein tagged by mVenus fluorescent protein and mRFP1 fluorescent protein. The lifetime is calculated for mVenus emission. The bar represents $10 \mu\text{m}$. (c) Corresponding fluorescence decay calculated over the whole image. The red curve represents the calculated instrument response function (IRF), and the gray curve represents measured decay data.

2.3 Anisotropy imaging

In the anisotropy measurement, polarized light is used for the excitation of the sample. The emission radiation is then divided into a component parallel I_{\parallel}

and a component perpendicular I_{\perp} to the polarization of the excitation beam. Subsequently, the anisotropy quantity $r(t)$ is defined as:

$$r(t) = \frac{I_{\parallel} - I_{\perp}(t)}{I_{\parallel} + 2I_{\perp}(t)} \quad (2.9)$$

The method is based on the preferential excitation of absorption moments aligned along the polarization of the excitation beam. This phenomenon is called photoselection. Subsequently, the light emitted by the molecule is also polarized when excited by polarized light.

However, there are several processes causing emission depolarization. One of them is the rotation of the molecule's transition moment axis caused by the diffusive rotation of the molecule while in an excited state. The rotational diffusion rate depends on the solvent viscosity and the size and shape of the rotating molecule. Thus when any of those parameters change, fluorescence anisotropy changes as well. This makes the anisotropy measurements suitable for the study of membrane fluidity [38], cell-interior viscosity [39], and protein-ligand interactions [40, 41].

Another of the most common cause of the depolarization of the emitted radiation is the non-zero angle between absorption and emission transition moments and homoFRET [42]. Resonance energy transfer causes additional displacement of emission transition moment and therefore causes a decrease in fluorescence anisotropy.

Depolarization happens in time and is manifested by anisotropy decay:

$$r(t) = r_0 \cdot \exp(-k_{dep}t), \quad (2.10)$$

where r_0 is time-zero anisotropy, a limiting anisotropy determined in the absence of depolarizing influences (when absorption and emission transition moments are colinear, the value of time-zero anisotropy is 0.4 [4]) and k_{dep} is the rate of depolarization.

Anisotropy measurements can be performed in two different modes - time-resolved and steady-state. In time-resolved measurements, an anisotropy decay is obtained from eq. 2.9. The steady-state anisotropy is calculated as an average anisotropy weighted over an overall intensity:

$$r = \frac{\int_0^{\infty} r(t)I(t)}{\int_0^{\infty} I(t)}, \quad (2.11)$$

or analogously by calculating stationary intensities I_{\parallel} , I_{\perp} and using the formula:

$$r = \frac{I_{\parallel} - I_{\perp}}{I_{\parallel} + 2I_{\perp}}. \quad (2.12)$$

The quantitative influence of depolarization factors on anisotropy is given by a simple relationship known as Soillelet's rule:

$$r = r_0 \prod_i d_i \quad (2.13)$$

where d_i represents the decrease in anisotropy caused by individual depolarization factors (a specific example of this rule can be found in [4]).

In this thesis, the anisotropy measurements were used to study protein homooligomerization. Steady-state anisotropy was evaluated at selected regions within fluorescently labeled cells; subsequently, the cells were photobleached so that the concentration of active fluorescent acceptor decreased to 30 % of the initial concentration. After that, anisotropy was re-evaluated within the same region. The decrease in the amount of fluorescently active acceptors causes a decrease in homoFRET. Thus an increase in steady-state anisotropy should be observed. If fluorophores or fluorophore-labeled proteins did not form an oligomer or the mean fluorophore-to-fluorophore distance was too big, homoFRET would not occur. Therefore, we should not observe a change in anisotropy after bleaching the acceptor. The experimental setup for anisotropy measurements is described in Chapter 3.2.

2.4 Fluorescent proteins

Fluorescent proteins are a class of proteins capable of spontaneously forming a fluorescent chromophore. Thanks to this and the simple application of genetic engineering methods, these proteins can serve as fluorescent probes.

The first discovered fluorescence protein was co-called green fluorescent protein (GFP). It was purified from the bioluminescent jellyfish *Aequorea victoria* in 1962, cloned in 1992, and finally expressed in living organisms in 1992 [43, 6]. Since then, many different mutants of wild-type GFP (wtGFP) have been engineered. Mutations provide GFP variants with improved spectral characteristics such as shifted excitation peak, increased quantum yield, and mainly increased photostability. Other natural fluorescent proteins can be found in corals and are often called red fluorescent proteins (RFPs).

In this work, mVenus and mRFP1 fluorescent proteins were used as fluorescent labels - their lifetimes and anisotropy were used for studying the oligomerization of labeled proteins. mVenus is a monomeric rapidly-maturing yellow fluorescent protein derived from *Aequorea victoria*, published in 2006 [44]. mRFP1 is a monomeric, slowly maturing red fluorescent protein derived from *Discosoma sp.* published in 2002 [44].

Because of its spectrum characteristics, mRFP1 can be used as an acceptor with the mVenus donor in heteroFRET experiments. The emission and excitation spectra of both used fluorescent proteins can be found in Fig.2.3.

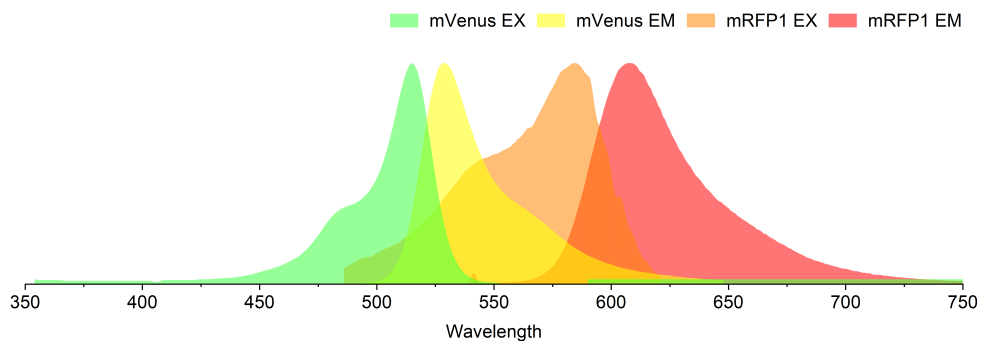


Figure 2.3: The emission and excitation spectra of mVenus and mRFP1 heteroFRET fluorescent protein pair (taken from the FPBase database [45])

3. Samples and methods

3.1 Sample preparation

This work studied the p53 protein in its wild type and mutated (L344P) form and the nucleophosmin protein in its wild type and mutated form and their mutual interactions. This chapter describes basic gen engineering techniques used to prepare the samples with needed proteins. All samples were prepared in the Institute of Hematology and Blood Transfusion by the research partner Aleš Holoubek, Ph.D.

3.1.1 Cell cultivation and plasmid transfections

HEK-293T cells were seeded to the cell density of 1×10^5 ml 24 h prior to transfection. Transfection was achieved with jetPrime transfection reagent (Polyplus transfection) following the manufacturer's protocol. The growth medium was replaced 4 h after the transfection, and cells were further grown for 20 to 40 hours before analysis.

3.1.2 Plasmid construction

Plasmids containing fluorescent protein fusions were prepared by standard molecular cloning techniques.

Plasmids for the mVenus-labeled NPM variants production were subsequently prepared in [46] using the constructed pmVenus-C1. Constructs with mRFP1 were already prepared in previous studies: [47] (fusion of mRFP1 with NPMwt, NPMmut) and [48] (mRFP1 and NPMcut fusion).

For this diploma thesis, plasmids for producing fluorescently labeled p53 variants were constructed on the original pmRFP1-C2:p53wt vector [13]. DNA fragment corresponding to specific TP53 transcript, isoform a (RefSeq. NM 000546.6, from NCBI database), was PCR-amplified from the pmRFP1-C2:p53wt plasmid using appropriate extended primers. Subsequently, it was sub-cloned to the vector pmVenus-C1 [46] using XhoI and BamHI unique restriction sites (Thermo Scientific) and T4 DNA ligase (NEB).

Next, TP53 sequence alteration leading to the L344P mutation was introduced to the pmVenus-C1:p53wt construct by Q5 Site-Directed mutagenesis kit (NEB). The DNA fragment with the altered sequence was again PCR-amplified using appropriate extended primers and reversely subcloned back to the pmRFP1-C2 vector. The whole process is summarized in a scheme in Fig.3.1.

All constructed plasmids were amplified in TOP10 E. coli competent cells (ThermoFisher Scientific), then purified with the PureYield Plasmid Miniprep System (Promega).

3.2 Microscopy - technical equipment

FLIM and anisotropy experiments were performed using an inverted IX83 microscope (Olympus, Tokyo, Japan) in a confocal mode (for the microscope scheme,

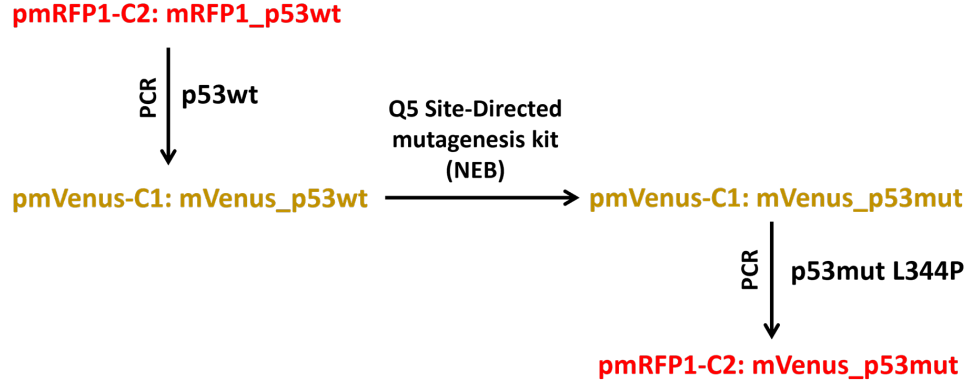


Figure 3.1: Scheme of stepwise preparation of plasmids including p53mut molecular cloning.

see Fig. 3.2). The microscope was equipped with a cell-cultivation chamber (Okolab, Pozzuoli, NA, Italy), which kept the chamber temperature at 37 °C to perform in-vivo experiments.

For fluorophores excitation, two lasers were used, pulsed 488 nm LDH-D-C(later), operating either at 20 MHz or 40 Mhz rate, and continuous 561 nm laser. Depending on the laser used, either a DM405/488/559/635 dichroic mirror or a DM561 dichroic mirror was used (both Olympus). Exceptionally, BS 20/80 beamsplitter was used for bright samples during anisotropy measurement in a red spectral region (Olympus).

The first experiments were performed using the UPLSAPO60x water immersion objective (Olympus) - NA = 1.2, which was later replaced by UPLSAPO30XS oil immersion objective¹ (Olympus) due to a smaller numerical aperture - NA = 1.05 - causing less artificial depolarization.

The emission path was different for FLIM and anisotropy experiments. In FLIM mode, the emission light passes through a Semrock 534/30 or a 520/35 bandpass filter to the cooled hybrid photomultiplier (PMT) with a GaAsP photocathode (PicoQuant).

In the anisotropy mode, the light is divided by a polarization beamsplitter (PicoQuant add-on) into two components - one with parallel and one with perpendicular polarization (with respect to the original light source). Subsequently, each component passes through a single Semrock 534/30 bandpass filter and continues to the cooled hybrid GaAsP detector.

Filters have been labeled and assigned to the individual detector within one measurement day to avoid mismatching. Labeling within two or more measurement days was unnecessary since the microscope was calibrated each day.

3.3 Measurement calibration

Since the signals from two intensity detectors (parallel and perpendicular emission intensity compound) need to be combined for anisotropy measurements, it is

¹It is important always to wipe the bottom of the Petri dish that contains the sample cells properly to avoid optical artifacts when working with both types of immersion.

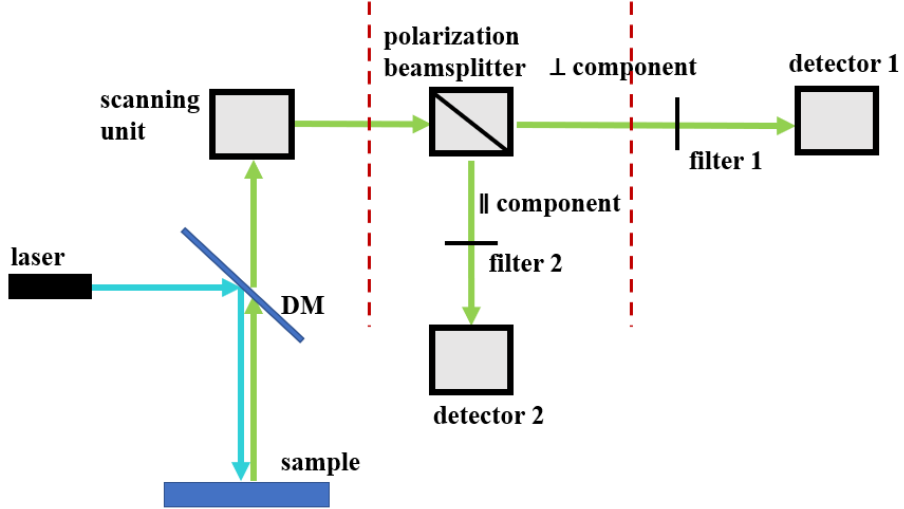


Figure 3.2: The simplified ray path scheme. Cyan lines represent excitation rays, while green lines represent emission rays. Dashed red lines divide the additional anisotropy part of the experiment from the FLIM part.

necessary to calibrate detector channels to the same sensitivity. We incorporate the so-called G-factor into the relationship for anisotropy as follows:

$$r(t) = \frac{I_{\parallel}(t) - GI_{\perp}(t)}{I_{\parallel}(t) + 2GI_{\perp}(t)}. \quad (3.1)$$

Since the sensitivity of the detectors is spectrally dependent, the G factor is a quantity that changes when different filters are used, and it is necessary to determine it repeatedly for each experimental setup.

To determine the G-factor, we measured the anisotropy of a drop of fluorescein solution in distilled water and ethanol. Fluorescein is a small molecule with fast rotation (the rotational correlation time in an aqueous (non-viscous) medium is ≈ 200 ps [49], while the lifetime of the excited state is ≈ 3.9 ns [50]). After excitation, we, therefore, expect a rapid depolarization of the excited radiation, i.e., zero steady-state anisotropy. The G-factor is defined as the ratio of I_{\parallel} and I_{\perp} . The following figure sequence shows the procedure for determining the G-factor:

1. The intensity decay curves marked as I_{\parallel} and I_{\perp} are exported from Symphotime software.
2. A corresponding background is subtracted from both of the curves.
3. The area under both curves is calculated in the same time interval (usually, an interval from 3 to 30 ns was taken into account to avoid the depolarization process at the beginning of the curve and the messy background data at the end).
4. The G-factor is finally obtained by dividing these areas (integrals of the curves).

After multiplying the I_{\perp} by the G-factor, we should get two converging curves, which proves the procedure was performed correctly.

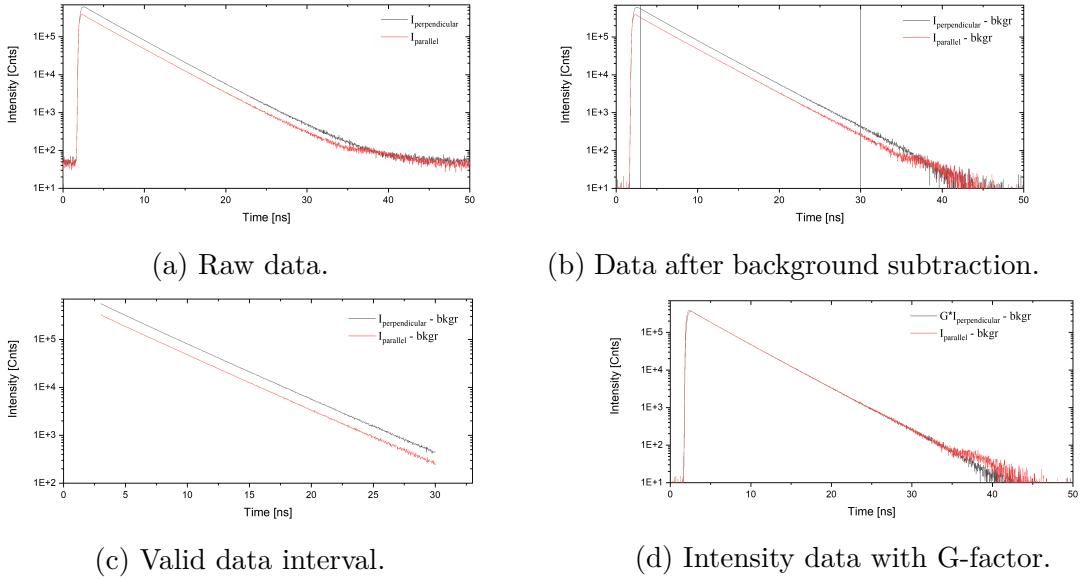


Figure 3.3: G-factor determining procedure. (a) Raw intensity data (b) Intensity data after background subtraction. (c) Chosen data interval for integration. (d) Converging intensity curves after G-factor correction.

A quicker way to determine the G-factor is by working directly in the `SymphoTime` software anisotropy imaging mode, where the background intensity to the pixel can be set, and zero steady-state anisotropy is achieved by manipulating the G-factor value. Both methods have been tried with the same results, so a faster method was used henceforward.

3.4 Data acquisition and processing

3.4.1 HeteroFRET experiments (FLIM measurement)

For heteroFRET experiments, FLIM measurements are performed in the following steps:

1. Find the cells containing both donor and acceptor fluorescent proteins and perform the FLIM measurement.
2. Photobleach the acceptor in the chosen cell/s by irradiating them with full laser intensity.
3. Perform FLIM measurement of the same cells.

An increment in the donor lifetime should be observed after the acceptor photodestruction since the heteroFRET should be prevented. A demonstrable change in the donor lifetime is considered to be $\Delta\tau > 0.04$ ns.

Lifetime over a region of interest is calculated in `SymphoTime` software using bi-exponential reconvolution with calculated instrument response function (IRF):

$$y(t) = \sum_{i=1}^2 \text{IRF} \otimes A[i] \exp \frac{t}{\tau[i]} + \text{Bkg}_{\text{rDec}} \quad (3.2)$$

Intensity averaged lifetime τ_{AvInt} is then used for lifetime comparison:

$$\tau_{AvInt} = \sum_{n=0}^1 \frac{I_n \tau_n}{I_{sum}} \quad (3.3)$$

In the results of the heteroFRET measurement, the images show the intensity image of the donor, the intensity image of the acceptor, the ratio of these intensity images in a logarithmic scale, and the image with the lifetime contrast. Lifetime values averaged over cell region are shown in the lifetime image beside the corresponding cells. The first row represents the initial state of the sample, and the second row represents the state after the total photobleaching of the acceptor in the area bounded by a white line using the 561 nm continuous laser. Scale bars in all images represent 10 μm . Color map images contain calibration bars.

3.4.2 HomoFRET experiments (steady-state and time resolved anisotropy measurement)

For homoFRET experiments, anisotropy measurements were performed following the procedure:

1. Find the cells with a fluorescent protein and perform an anisotropy measurement.
2. Photobleach the fluorescent protein in a chosen cell/s to 30 % of its original intensity to photodestruct a sufficient amount of protein that might have served as a homoFRET acceptor. For this use, do not use the laser at full intensity.
3. Perform an anisotropy measurement of the same cells.

An increase in a steady-state anisotropy of the photobleached cell/s indicates the suppressed homoFRET.

Steady-state anisotropy is calculated by `SymphoTime64` software after inputting G-factor value, background values for both measuring channels (perpendicular and parallel polarization channel), and threshold counts per pixel. It is possible to choose a region of interest and obtain average steady-state anisotropy and a histogram of anisotropy values inside this chosen region. Standard deviation was obtained using Gaussian fit for anisotropy distribution in program `Origin`. Steady-state anisotropy images are exported from `SymphoTime64` software as `.tif` and further processed in `Fiji` software for scale bar and calibration bar addition or contrast enhancement.

For time resolved anisotropy ROI analysis, channel 1 (perpendicular) and channel 2 (parallel) time resolved intensities were exported from `SymphoTime64` software and further processed in `Origin`. Background values were subtracted, and the formula for anisotropy calculation 2.9 was applied. Next, we set time 0 for the IRF maximum.

Plotted time-resolved anisotropy thus obtained was further fitted by the bi-exponential model:

$$r(t) = r_{\infty} + A_1 \exp(-t/\phi_1) + A_2 \exp(-t/\phi_2) \quad (3.4)$$

where t is time, r_∞ constant that mirrors molecule mobility restriction, A_1 , A_2 are exponential amplitudes, and ϕ_1 , ϕ_2 are rotational correlation times. Typically rotational correlation time is the average time a molecule needs to rotate one radian, and it is given by the Einstein-Stokes relation:

$$\phi = \frac{\eta V}{kT} \quad (3.5)$$

where η is a dynamic viscosity of molecule microenvironment, V rotating molecule volume, k the Boltzman constant and T is the molecule microenvironment temperature.

When molecule rotation is the only factor causing light depolarization, ϕ is related to the depolarization rate constant as $k_{dep} = 1/\phi$. Besides this, we use the term rotational correlation time to describe various depolarization causes. ϕ_1 and ϕ_2 correspond to the fast depolarization caused by homoFRET and slow depolarization caused by rotation of the whole molecule, respectively. ϕ_2 was approximately determined using relation 3.5 adjusted for specific volume \bar{v} and hydration h of the studied protein:

$$\phi = \frac{\eta M}{RT}(\bar{v} + h) \quad (3.6)$$

where M is the molecular weight of a fluorophore, and R is the ideal gas constant. We assumed $\bar{v} = 0.75$ ml/g, $T = 37$ °C, $\eta(37$ °C) = 0.69 cP and hydration $h = 0.2$ (as considered in [46]).

As fitting, we considered p53wt to be in the form of a dimer, p53mut a monomer, NPMmut a pentamer, and NPMmutcut a monomer. To every monomer unit, we assumed one fluorescent tag was attached. Molecular weights of protein monomers were considered as follows: $M_{p53} = 44$ kDa, $M_{NPM} = 35$ kDa and $M_{mVenus} = 27$ kDa. Following ϕ_2 were therefore assumed for fitting:

- $\phi_2 = 36$ ns for p53wt tagged by mVenus
- $\phi_2 = 18$ ns for p53mut tagged by mVenus
- $\phi_2 = 77$ ns for NPMmut tagged by mVenus
- $\phi_2 = 16$ ns for NPMcut tagged by mVenus

Variables in eq.3.4 should comply following formula:

$$r_0 = r_\infty + \sum A_i \quad (3.7)$$

where r_0 is the limiting anisotropy given for every fluorophore.

However, a large amount of noise in the data often causes big inaccuracy of bi-exponential fitting, so the fit is often complemented by third exponential decay characterized by A_3 and t_3 coefficient. A new parameter A^* defined as $A^* = A_1 + A_3$ is introduced to represent the homoFRET.

After fitting both anisotropy decay - before and after photobleaching - amplitudes of fast and slow depolarization components (A_1 and A_2 , respectively) of the bi- or tri-exponential model are compared. Suppose there is a homoFRET in the given sample. In that case, an increase in A_2 and a decrease in A_1 is expected

after photobleaching as slow depolarization caused by molecule rotation becomes prevalent.

Fitting is performed in program `Origin` using global fitting that ensures the same rotational correlation times and r_∞ for the state before and after fitting.

For clarity, figures showing the results of the homoFRET measurements will have the same structure if not said otherwise. The figures will show the intensity of combined perpendicular and parallel components of the mVenus fluorescence signal filtered by 534/35 bandpass filters fluorescent protein in green color followed by anisotropy images measured using 482 nm pulsed laser excitation. Steady-state anisotropy values averaged over the individual cells will be written into anisotropy figures altogether with the calibration bar. The first row will represent the initial state of the sample, and the second row the state after 488 nm photobleaching of the cell in a white circle to 30 % of its initial intensity. The scale bar in the figures will always represent 10 μm . The top-right image will contain plotted steady-state anisotropy distribution over ROI before (orange) and after (blue) photobleaching. The bottom-right image will contain ROI anisotropy decay before (orange) and after (blue) photobleaching, with the black lines representing corresponding decay fits.

4. Results

This chapter discusses technical differences and results of the individual carried out experiments. Sections are divided according to the studied proteins.

Firstly, experiments concerning solely the p53wt and p53mut proteins are gradually summarized. Secondly, NPMcut experiments are summarized followed by experiments investigating the mutual interaction of p53 proteins (labeled with mVenus) and NPM proteins (labeled with mRFP1) and their homo-oligomeric state during the interaction. In the case of NPMmut the same experiments with the opposite tagging are presented too. Concerning work on the thesis, the measurements in sections do not always follow each other in time.

During the experiments, an error was detected in the mVenus-tagged p53mut construct production. Results concerning faulty construct are not published in the thesis since they might cause confusion.

4.1 p53 variants

Experiments with p53 proteins aim to verify assumptions from the literature about the oligomerization state of these proteins in living cells and to investigate the mutual interaction of p53wt and p53mut proteins.

4.1.1 p53wt

Experiments began with the protein p53wt, which was proved to form oligomers [51]. Two types of samples were prepared, one for heteroFRET and one for the homoFRET experiment. HeteroFRET samples contained p53wt tagged with a yellow fluorescent protein mVenus and p53wt protein tagged with a red fluorescent protein mRFP1, while homoFRET samples contained only p53wt marked with the mVenus protein.

HeteroFRET lifetime measurements followed the procedure described in Section 3.4. Chosen cells were bleached by a 561 nm laser, and lifetime was measured before and after bleaching. Photobleaching should be responsible for acceptor photodestruction, which prevents heteroFRET from happening. Without the possibility of the non-radiative energy transfer, fluorophore molecules remain in the excited state longer, which is reflected in an increase in their lifetime.

Lifetime change of about $\Delta\tau = (0.10 \pm 0.02)$ ns in all bleached cells confirmed the presence of heteroFRET and, therefore, a probable oligomerization of p53wt. Representative processed measurement - fluorescent protein intensities, the logarithm of their ratio, and calculated lifetime images - is shown in Fig.4.1. Lifetime values averaged over the cell can be found near the corresponding cells in the lifetime images, altogether with a lifetime color scale. A white circle borders the bleached area. We can see that in this measurement lifetime rose from $\tau = 2.74$ ns to $\tau = 2.86$ ns resulting in lifetime change $\Delta\tau = 0.12$ ns, which is considered significant.

HomoFRET experiments followed the basic procedure described in Section 3.4. The steady-state anisotropy difference between the bleached and initial state of the cell was $\Delta r = (0.03 - 0.05)$, also indicating an energy transfer. The results of

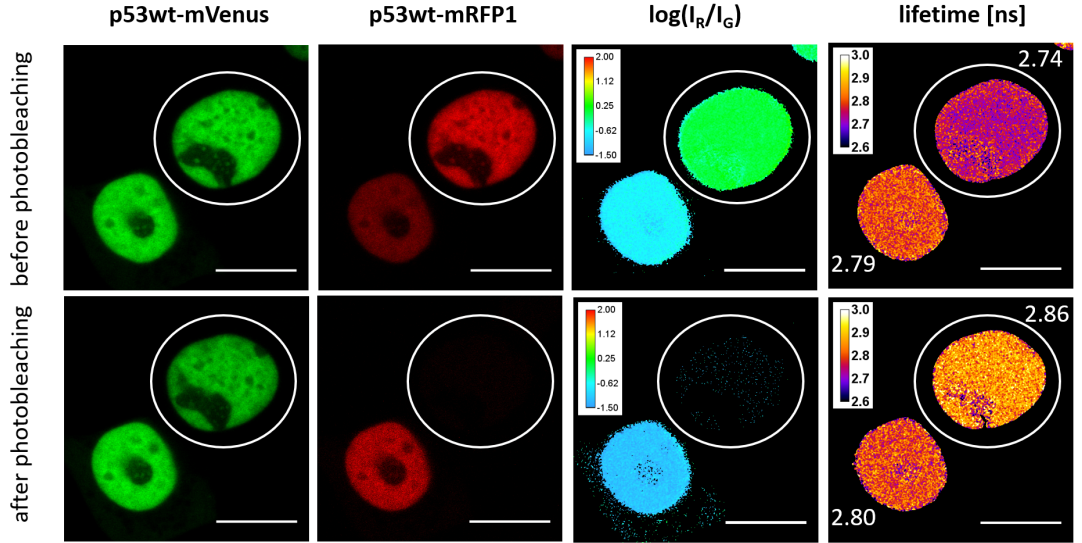


Figure 4.1: p53wt heteroFRET measurement. HEK-293T cells containing p53wt labeled with mVenus and p53wt labeled with mRFP1 fluorescent protein.

a representative measurement are shown in Fig.4.2. From the anisotropy image and anisotropy distributions, the shift in ROI's anisotropy is evident - steady-state anisotropy changed from $r = 0.26$ to $r = 0.31$, while the anisotropy of an unbleached cell remained unchanged.

Anisotropy decay curves were obtained as described in subsection 3.4.2 using a corresponding G-factor and fitted by bi-exponential decay according to 3.4. By investigating these anisotropy decay curves, it is evident that the fast component prevails in the anisotropy decay of the initial state, while in the state after the photobleaching, it has a smaller contribution. Parameter A_1 corresponding to the fast decaying exponential is equal to 0.20 ± 0.01 before and $A_1 = 0.07 \pm 0.01$ after photobleaching. Parameter A_2 corresponding to the slower decaying exponential is equal to 0.15 ± 0.01 before photobleaching and $A_2 = 0.29 \pm 0.01$ after photobleaching. By comparing these parameters before and after photobleaching, we can conclude that homoFRET transfer was present and subsequently reduced by photobleaching. HomoFRET experiments, therefore, conclude the oligomeric state of p53wt, which is in agreement with heteroFRET experiments.

4.1.2 p53mut

Next, p53mut heteroFRET and homoFRET experiments were performed. According to the literature ([14]), no or small change in lifetime and anisotropy has been expected as the protein is expected to be monomeric.

HeteroFRET experiments were performed using mVenus fluorescent protein as a donor and mRFP1 fluorescent protein as an acceptor. Representative measurement is shown in Fig.4.3. The observed change in a bleached cells' lifetime was in the interval $\Delta\tau = (0.03 - 0.05)$ ns and seems to be related to the ratio of acceptor to the donor. Such a change in lifetime is the threshold for determining the presence of heteroFRET, so the results do not appear to be as conclusive as expected, and it is possible that some proteins do not exist in monomeric but

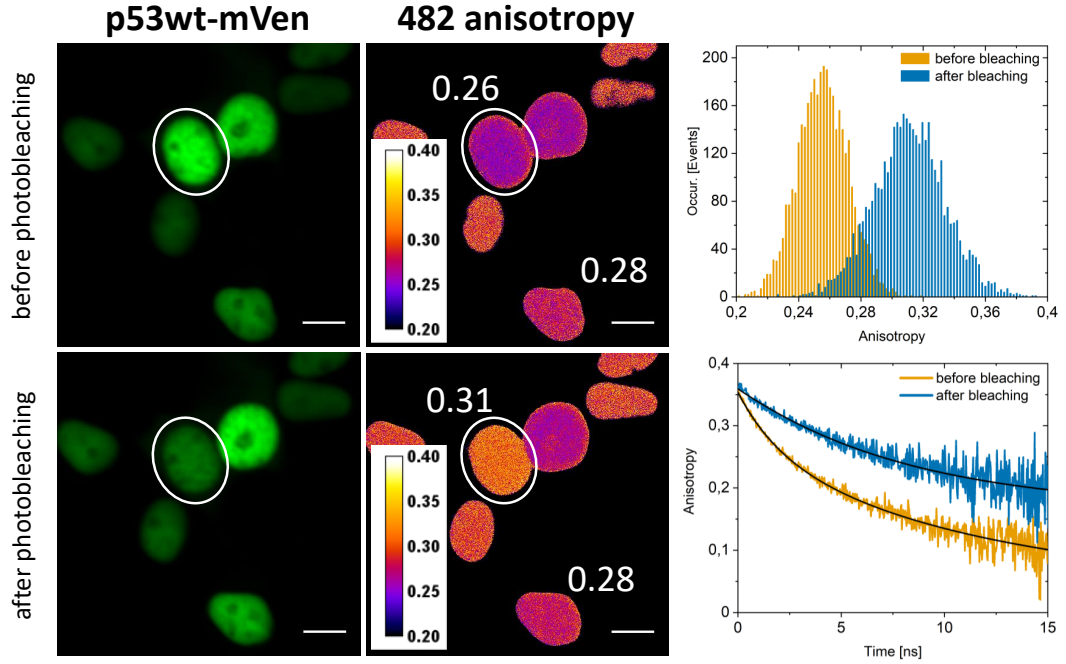


Figure 4.2: mVenus-tagged p53wt homoFRET measurement.

rather oligomeric form. The change in the lifetime was compared in a Tukey's range test performed in the Origin2020 software (using app *Paired comparison plot*), where unbleached cells were used as an unchanging reference. The result of this test is shown in Fig.4.4 along with the pairwise test result for the p53wt heteroFRET experiments for comparison. Lifetime changes for p53mut show a smaller degree of significance than for p53wt.

Subsequently, homoFRET experiments were performed with p53mut tagged with mVenus - see Fig.4.5.

The change in anisotropy in five bleached cells was in the interval of $\Delta r = (0.01 - 0.02)$ and appears to be related to the intensity of the fluorescent tag (proportional to its concentration). The cell containing a higher level of the fluorescent protein shows a larger change in anisotropy. Also, anisotropy, in general, appears to be lower for a less bright cell (not taking into account cells with an insufficient signal).

Anisotropy changes from all performed measurements were again compared through Tukey's range test. Results are shown in Fig.4.6. The significance of anisotropy change after the cell photobleaching is higher than that of lifetime changes in the p53mut heteroFRET experiment, which might implicate homoFRET experiments as more sensitive for protein interaction detection.

What is left to investigate are anisotropy decay curves. As shown in Fig.4.5, anisotropy decay appears to be flatter in opposition to p53wt (Fig.4.2). The value of the correlation time was first left as a fitting parameter, and the result of the fit turned out to be closer to the correlation time for the dimer than for the monomer. Therefore, the value of $\phi_2 = 36$ ns corresponding to the p53 dimer was used for the following bi-exponential global fit - fit results are summarized in A. The value of a slow component amplitude was $A_2 = 0.19 \pm 0.04$ before bleaching and $A_2 = 0.26 \pm 0.04$ after bleaching. The fast component had an amplitude

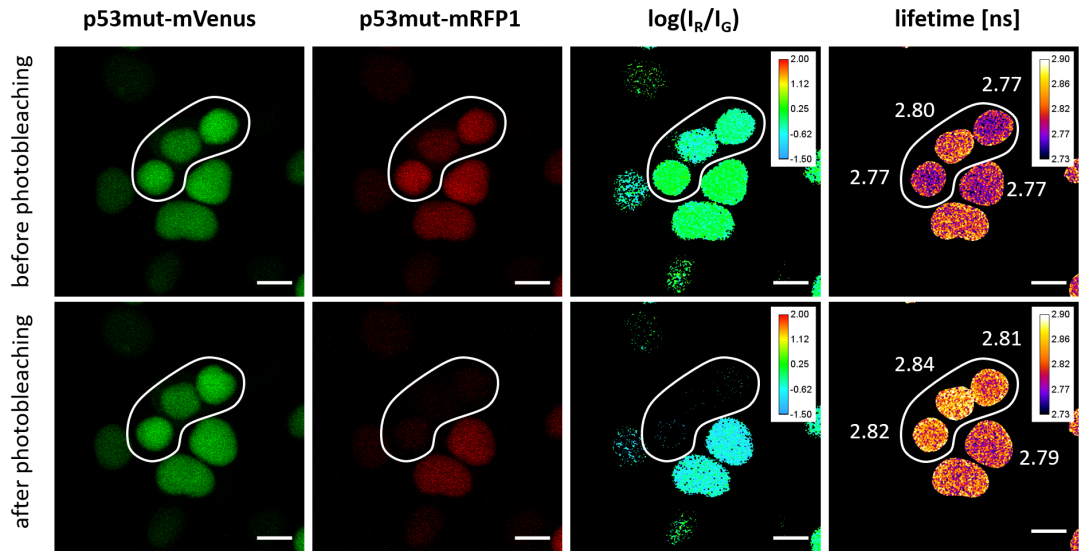


Figure 4.3: p53mut heteroFRET measurement. HEK-293T cells containing p53mut labeled with mVenus and p53wt labeled with mRFP1 fluorescent protein.

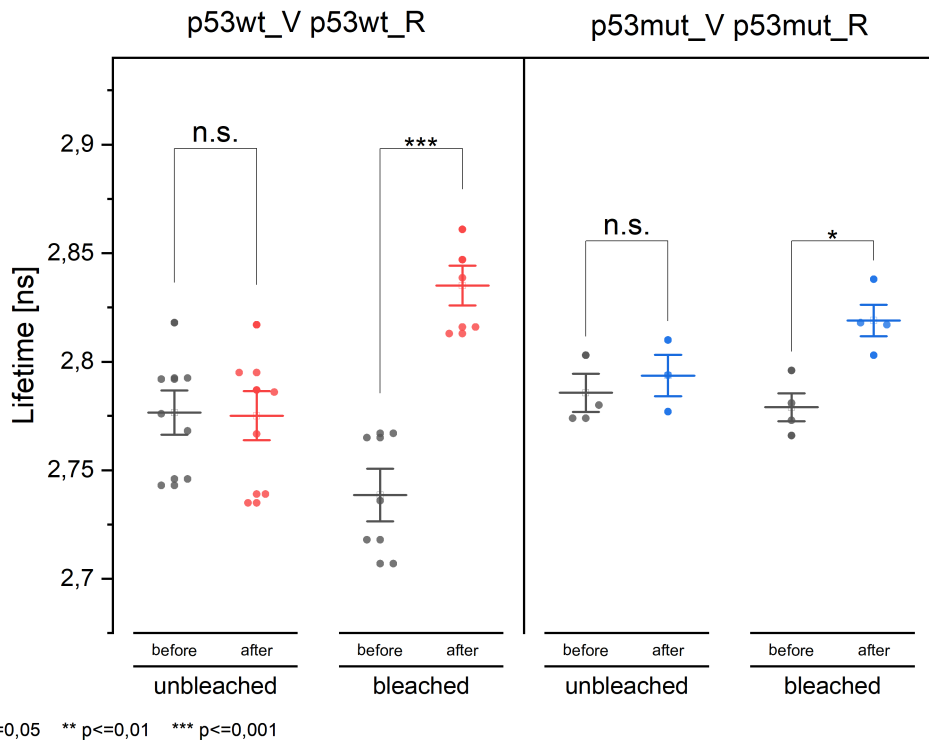


Figure 4.4: p53 heteroFRET Tukey's range test containing data from several heteroFRET measurements for p53wt and p53mut protein plotted using Origin app *Paired comparison plot*. Lifetime changes of unbleached cells in both constructs were used as non-significant (n.s.). The figure shows higher significance for p53wt lifetime changes compared to p53mut. Lifetime changes for p53mut are still considered significant. Fluorescent tags used were mVenus as a donor and mRFP1 as an acceptor.

$A_1 = 0.11 \pm 0.02$ before bleaching and $A_1 = 0.05 \pm 0.01$ after bleaching. A small change in both amplitudes indicates a weak interaction, also reflected in the steady-state anisotropy images.

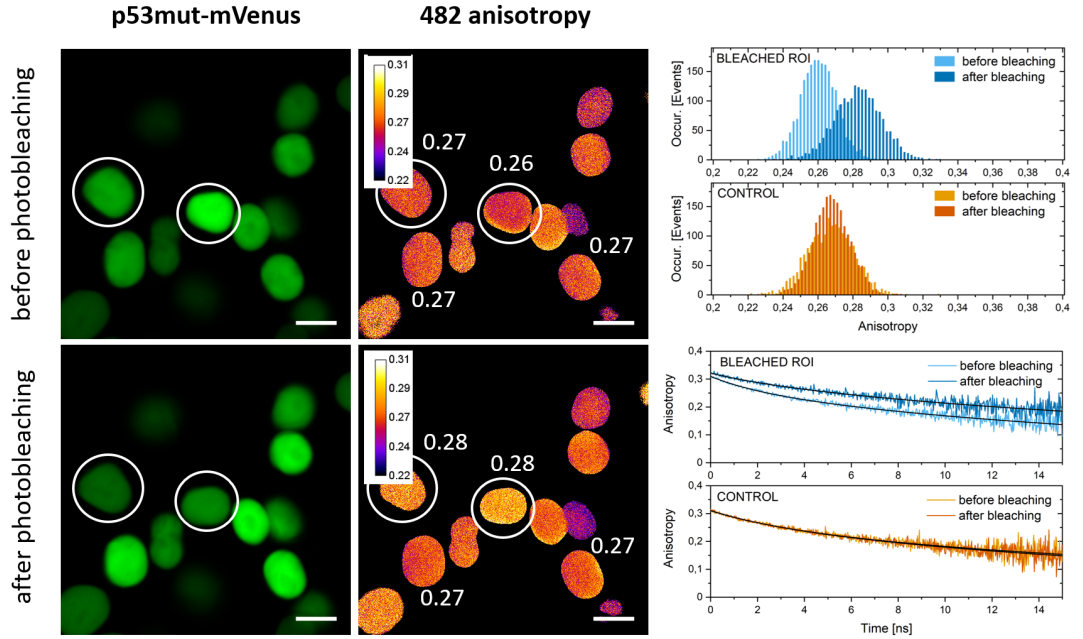


Figure 4.5: mVenus-tagged p53mut homoFRET measurement. Top-right image shows steady-state anisotropy distribution over bleached and unbleached ROI (marked as control). Bottom-right image contains anisotropy decays for bleached ROI and unbleached control.

4.1.3 mRFP1 labeled p53 constructs

Since we had at our disposal red-labeled p53mut, we decided to measure the anisotropy in the red spectral region and test the oligomeric properties of p53wt and p53mut again. Results of homoFRET experiments where mRFP1 is used as a fluorescent tag are shown in Fig.4.7 for p53wt and in Fig.4.8 for p53mut.

Images contain intensity images of combined perpendicular and parallel components of fluorescence signal filtered by 645/65 bandpass filters, calculated steady-state anisotropy images, and anisotropy distribution from the chosen ROIs before and after photobleaching. A white circles mark the bleached cells and draws attention to the relevant regions in calculated images. The scale bar represents 10 μm . Steady-state anisotropy values averaged over cell region are shown in the anisotropy images next to the corresponding cell. Calibration bars are also located in anisotropy images. Anisotropy distributions are taken from one of the bleached cells and from one of the unbleached cells (reference). Since we have no pulsed laser with a suitable wavelength for mRFP1 excitation in our laboratory, a 561 nm continuous laser was used as the excitation source. That is a reason why no anisotropy decay curve could be constructed.

Steady-state anisotropy change after bleaching is $\Delta r = 0.01$ in both prepared samples. Although the shift in the anisotropy distribution of the bleached cell for p53wt (Fig.4.7) appears to be slightly greater than in the case of p53mut

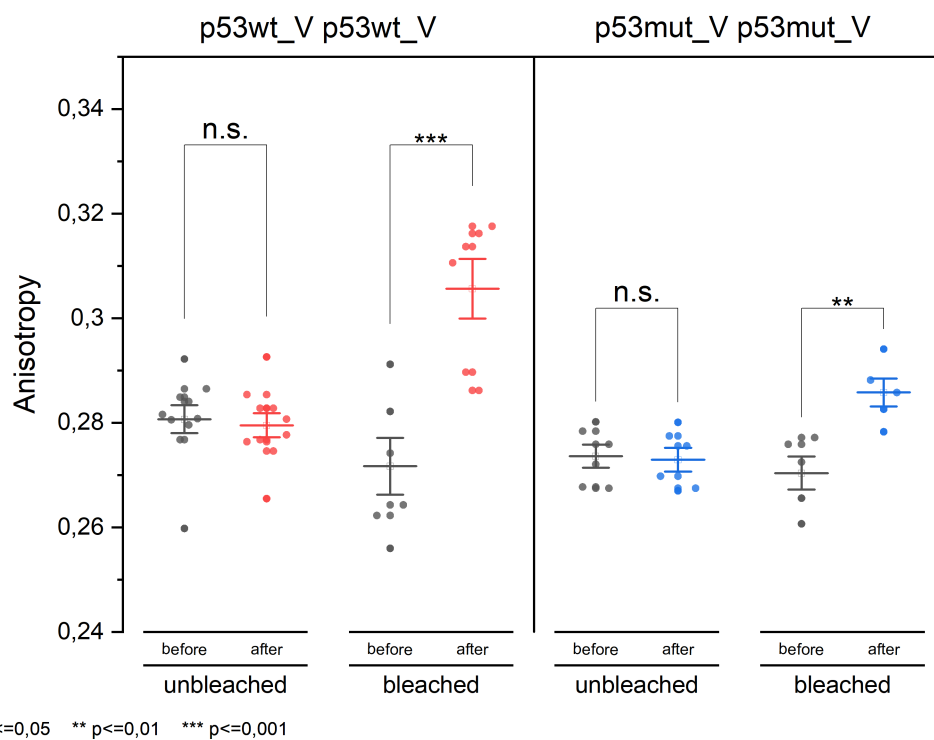


Figure 4.6: p53 homoFRET Tukey's range test containing data from several homoFRET measurements for p53wt and p53mut, both tagged with mVenus. Data are plotted using Origin app *Paired comparison plot*. Anisotropy changes of unbleached cells in both constructs were used as non-significant (n.s.). The figure shows higher significance for p53wt anisotropy changes compared to p53mut. Anisotropy changes for p53mut are still considered significant.

samples (Fig.4.8), this change is not significant enough within the margin of error to conclude anything besides the fact that mRFP1 is not suitable for our homoFRET experiments (more can be find in discussion).

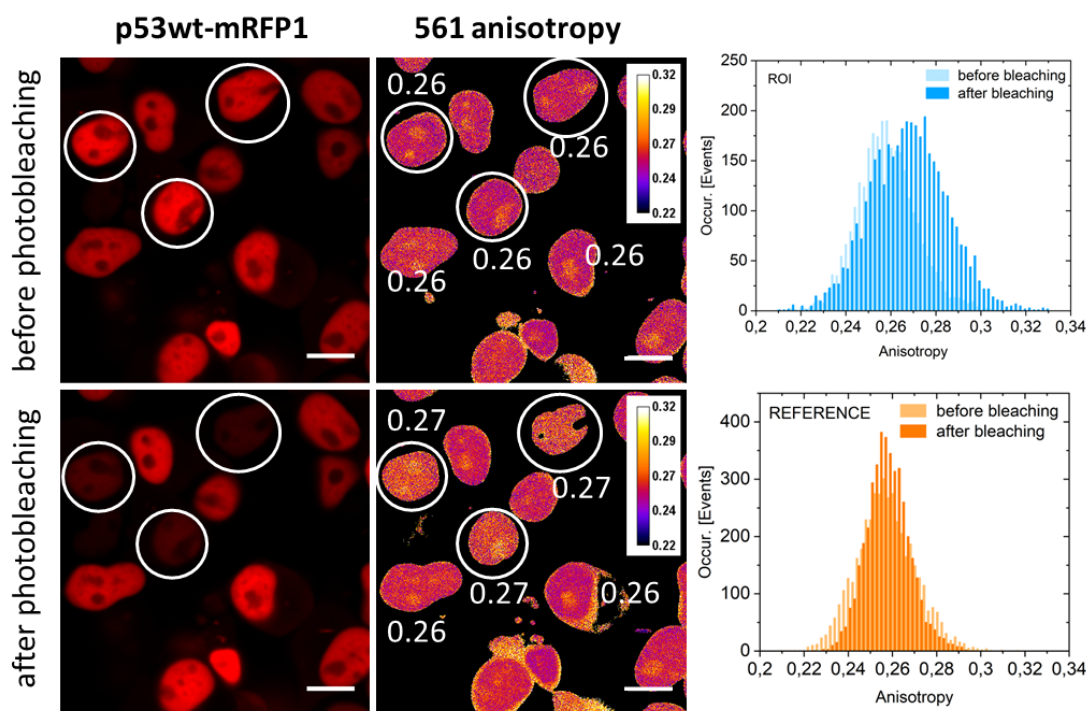


Figure 4.7: p53wt labeled with mRFP1 homoFRET experimet. Anisotropy distributions are shown for bleached (ROI) and unbleached cells (reference)

4.1.4 p53wt and p53mut interactions

Next step in investigating p53 proteins was to study heteroFRET between p53mut and p53wt. Experiments were performed using fluorescent tag mVenus at p53mut and mRFP1 tag at p53wt and vice versa. HeteroFRET results are shown in Fig.4.9 and Fig.4.10. Seeing localization of these two proteins next to each other we can notice that p53wt avoids nucleolus while p53mut is more evenly distributed throughout the nucleus and in the nucleoli. Lifetime changes in performed heteroFRET experiments were about $\Delta\tau = (0.05 - 0.06)$ ns when p53mut is tagged with a donor and $\Delta\tau = (0.06 - 0.08)$ ns when p53wt is tagged with a donor. Asymmetry when using the reversed labeling might be caused for example by different mutual orientation of the fluorescent labels when connected to one or the other studied protein, which affects the FRET. Despite the asymmetry both of the measurements show that wild type and L344P mutant p53 proteins could interact with each other in living cells.

4.2 NPMcut

NPMcut is an NPM protein without the oligomerization domain. HomoFRET experiments with this protein labeled with mVenus should not show any signif-

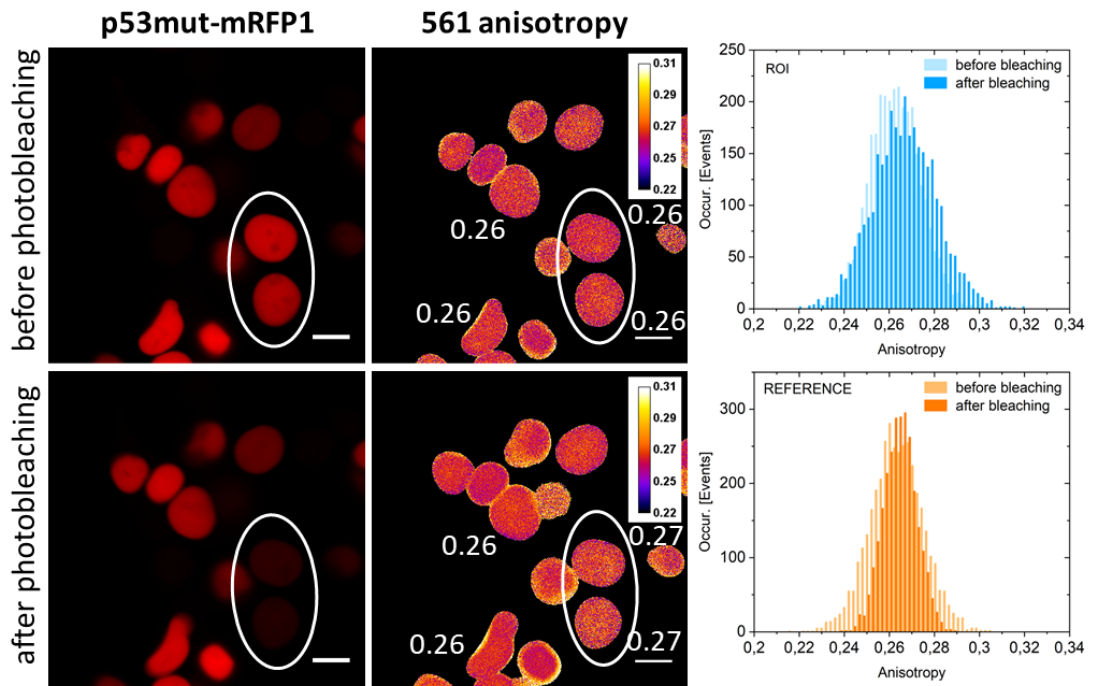


Figure 4.8: p53mut labeled with mRFP1 homoFRET experiment. Anisotropy distributions are shown for bleached (ROI) and unbleached cells (reference).

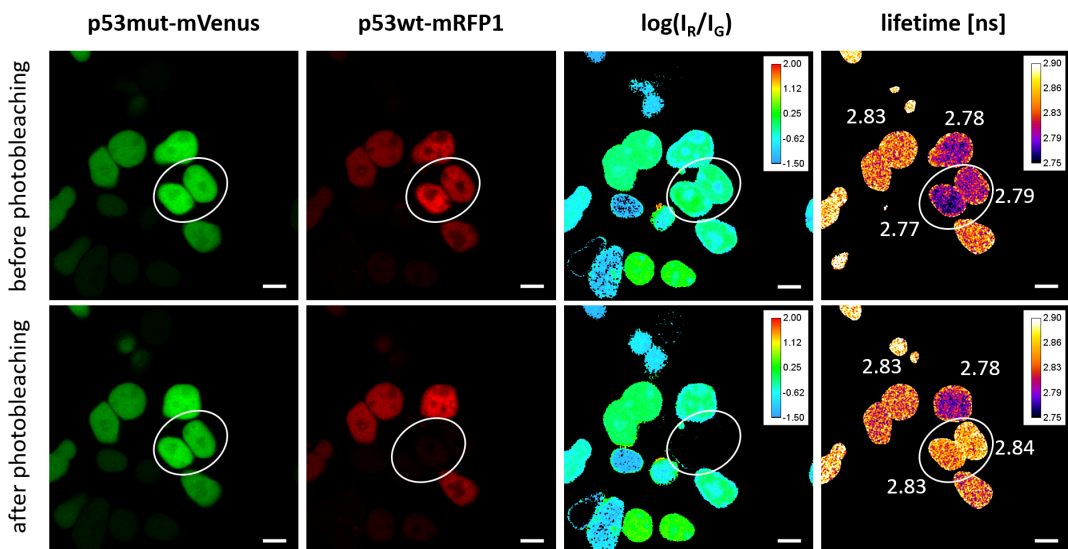


Figure 4.9: p53mut-p53wt heteroFRET measurement. HEK-293T cells containing p53mut tagged with mVenus and p53wt tagged with mRFP1 fluorescent protein.

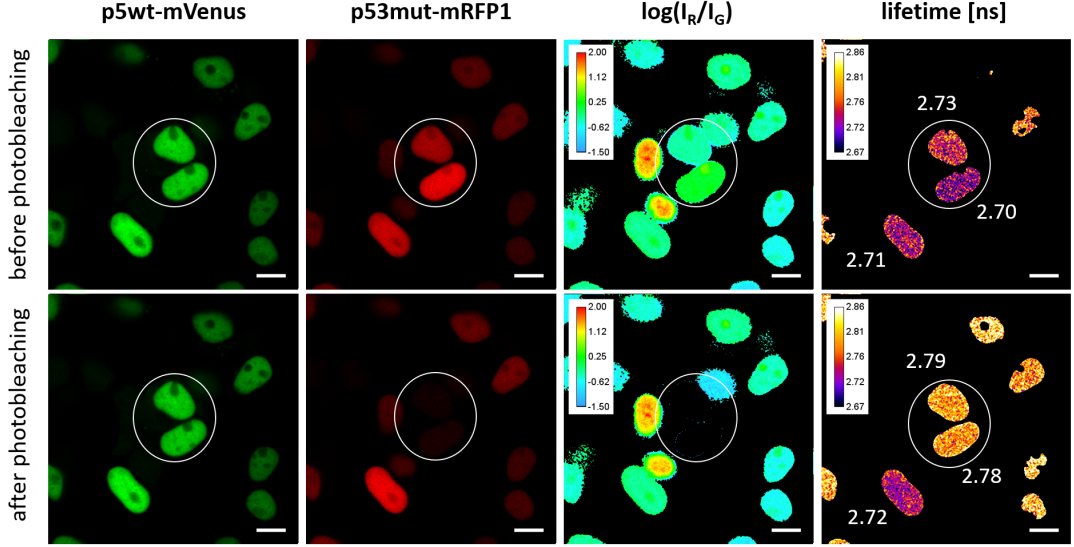


Figure 4.10: p53wt-p53mut heteroFRET measurement. HEK-293T cells containing p53wt tagged with mVenus and p53mut tagged with mRFP1 fluorescent protein.

icant anisotropy differences, and experiments should serve as a negative control as advised in previous work in our department [46].

We have performed several measurements on this sample with a conclusion that no change in the steady-state anisotropy was observed in less bright cells. In contrast, we can see anisotropy change a little in the measurements performed on bright cells like the one shown in Fig.4.11. The steady-state anisotropy value of the showed bleached cell before bleaching is $r = 0.29$, while after bleaching, it is $r = 0.31$. Anisotropy curves were difficult to fit while preserving the physical meaning of individual parameters. Curves showed the best fit when using bi-exponential decay with a corresponding ϕ_2 with a free absolute term. Amplitude corresponding to a slow decaying component $A_2 = 0 \pm 0.14$ before bleaching and $A_2 = 0.17 \pm 0.07$ after bleaching, while fast decaying component was $A_1 = 0.23 \pm 0.13$ before bleaching and $A_1 = 0.07 \pm 0.07$ after bleaching. Anisotropy decay before photobleaching appears to be mono-exponential with a correlation time $\phi_1 = 9 \pm 2$ ns (see Tab.A.1 in appendix) while anisotropy decay after photobleaching appears to be bi-exponential with a component corresponding to the slower correlation time $\phi_2 = 16$ ns prevailing.

We can only conclude that mVenus-labeled NPMcut did not prove to be a good negative control for our homoFRET measurements. The dependence of anisotropy change on cell intensity is a phenomenon already mentioned in p53mut homoFRET experiments where anisotropy decreases with a fluorescent protein concentration. This observation will be further discussed in Chapter 5.

4.3 NPM and p53 variants

In this chapter NPMmut and p53 protein interaction are studied. One of the aims was to determine the oligomerization state of p53 proteins during this interaction (the oligomerization state of NPM protein has already been determined).

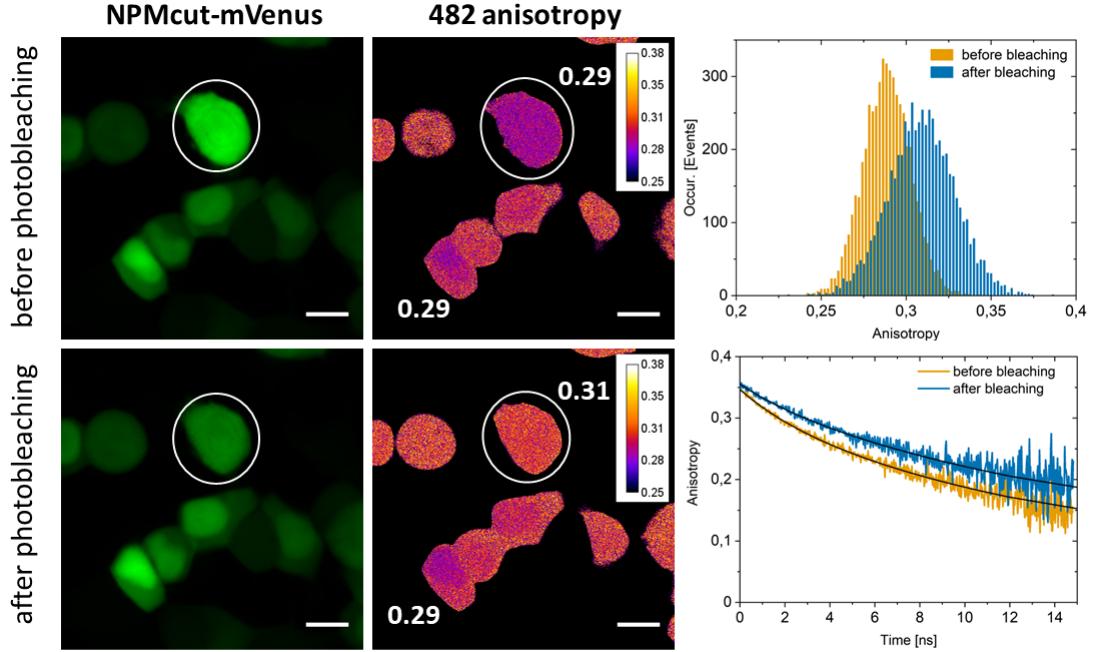


Figure 4.11: mVenus-tagged NPMcut homoFRET measurement.

In the previous work [13] p53wt was proven to be pulled out from nucleus to cytoplasm. In this work, we want to investigate whether the same process happens with p53mut.

4.3.1 NPMmut and p53wt

Since anisotropic measurements with a green laser excitation source were introduced in our workplace, we need to label the protein whose oligomerization state we want to investigate with the mVenus fluorescence tag. Therefore we first decided to use p53 proteins labeled with the mVenus and NPMmut labeled with mRFP1 in these experiments.

One of the performed experiments is shown in Fig.4.12 and Fig.4.13.

In these experiments, chosen cells were first bleached with a 561 nm laser to study p53wt-NPMmut heteroFRET. The same cells were afterward bleached by the 488 nm laser to 30 % of its initial intensity for p53wt homoFRET experiments.

From intensity images in Fig.4.12, which shows heteroFRET experiment, we can see that p53wt labeled with yellow fluorescent protein mVenus is pulled out of the nucleus into the cytoplasm where NPMmut tagged with mRFP1 is also located.

HomoFRET measurement of p53wt protein localized in the cytoplasm in the presence of NPMmut is shown in Fig.4.13. Anisotropy changes were usually $\Delta r = 0.03$, indicating that p53wt remains in oligomeric form while or after being pulled out of the nucleus. However, we do not know whether the dimer is part of the ternary complex.

Assuming p53 to be a dimer, the amplitude of the slow decaying component was $A_2 = 0.20 \pm 0.14$ before bleaching and $A_2 = 0.29 \pm 0.11$ after bleaching. The amplitude of the fast decaying component was $A_1 = 0.15 \pm 0.05$ before bleaching and $A_1 = 0.07 \pm 0.04$ after bleaching. The table with all the parameters of the

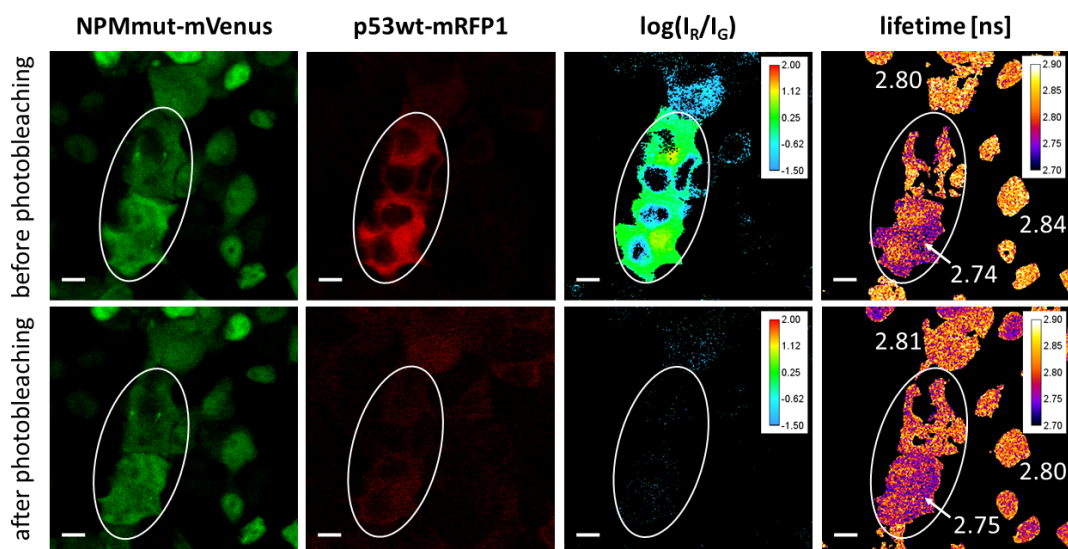


Figure 4.12: p53wt-NPMmut heteroFRET measurement. HEK-293T cells containing p53wt tagged with mVenus and NPMmut tagged with mRFP1 fluorescent protein.

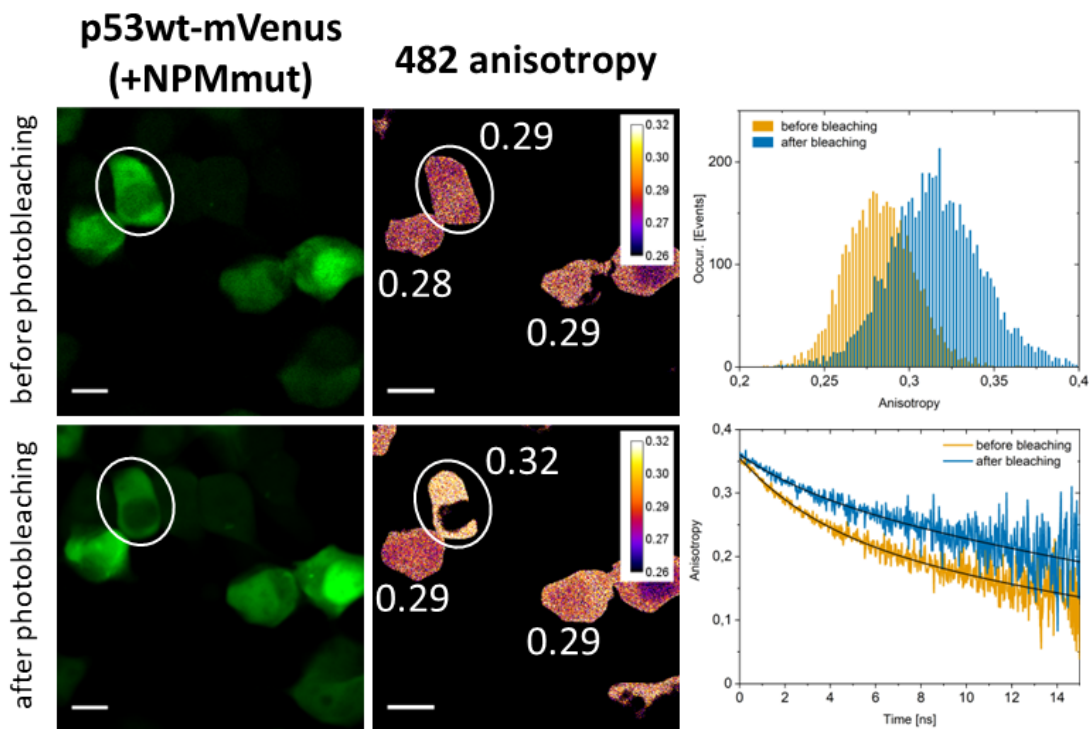


Figure 4.13: mVenus-tagged p53wt homoFRET measurement in the presence of NPMmut.

fit can be found in section A. It is necessary to note that the fit was clouded by a large error, probably caused by the noise in the data. However, a qualitative assessment of the change in the course of the anisotropy decay is visible to the naked eye.

As mentioned, results of the heteroFRET experiments of p53wt-NPMmut interaction are shown in Fig.4.12. Lifetime changes observed in these experiments were $\Delta\tau = (0 - 0.03)$ ns, which does not appear to be a significant change to prove protein interaction despite their common dislocation from the nucleus. However, after observing asymmetry in lifetime changes when studying p53wt-p53mut interactions, we have decided to perform experiments with reverse labeling for NPMmut and p53wt. One of those measurements is shown in Fig.4.14 and Fig.4.15.

Both NPMmut tagged with mVenus and p53wt tagged with mRFP1 are found in the cytoplasm as in the previous experiments. After mapping an initial state, the chosen cells were bleached by the 561 nm laser for heteroFRET measurement. Subsequently, some cells were bleached by the 488 nm laser to 30 % of their original intensity for NPMmut homoFRET measurement.

In Fig.4.14, we can see results of heteroFRET measurement with lifetime changes $\Delta\tau = 0.07$ ns. This change is significant enough to prove NPMmut and p53wt interaction in agreement with their co-localization and confirms the hypothesis of asymmetry of lifetime changes when reverse labeling is used.

Besides the asymmetry caused by reverse labeling, it is good to note that in experiments where p53wt was labeled with a mVenus donor, the measurements were unfortunately performed with weakly expressed proteins when we could observe the phenomenon of mRFP1 photoconversion. The mRFP1 fluorescent protein exhibits weak red-to-green photoconversion when exposed to strong excitation, and its lifetime is shorter than the lifetime of the mVenus fluorescent protein. In the case of cells showing a low intensity of mVenus or in the case of the cells where we bleached mVenus first, the signal of the converted mRFP1 might be reflected in the average lifetime of the given cell. This phenomenon must be taken into account in experiments performed on cells with a low fluorescent protein intensity and might contribute to the fact that none to small lifetime changes were observed in Fig.4.12.

In Fig.4.15, we can see the results of the NPMmut homoFRET experiment measured in a cell cytoplasm. Steady-state anisotropy was changed from $r = 0.21$ to $r = 0.27$, which makes Δr to be 0.05 and confirms the oligomeric state of NPMmut protein.

Decay curves showed the best global fit for the tri-exponential decay model where ϕ_2 was chosen to be constant according to 3.4.2 and the absolute term was set to zero. The amplitude of the slow decaying component before bleaching was $A_2 = 0.11 \pm 0.12$ while after bleaching, $A_2 = 0.20 \pm 0.12$. The amplitudes of the remaining two faster components had lower values in the state after bleaching; A_1 decreased from 0.11 ± 0.01 to 0.07 ± 0.01 , and A_3 decreased from 0.14 ± 0.02 to 0.09 ± 0.02 . A^* from A_1 and A_3 gives $A^* = 0.25 \pm 0.02$ before and $A^* = 0.16 \pm 0.02$ after photobleaching. The decrease in the combined amplitude of the fast components is compensated by the increase in the amplitude of the slow component, as expected for homoFRET using our model. The amplitudes are again clouded by the significant error discussed in Chapter 5.

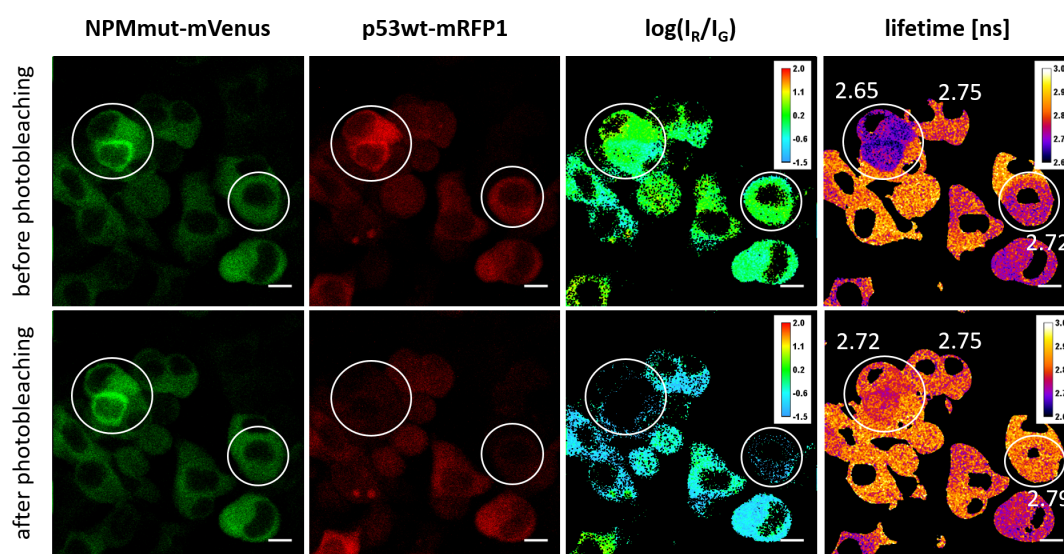


Figure 4.14: NPMmut-p53wt heteroFRET measurement. HEK-293T cells containing NPMmut tagged with mVenus and p53wt tagged with mRFP1 fluorescent protein.

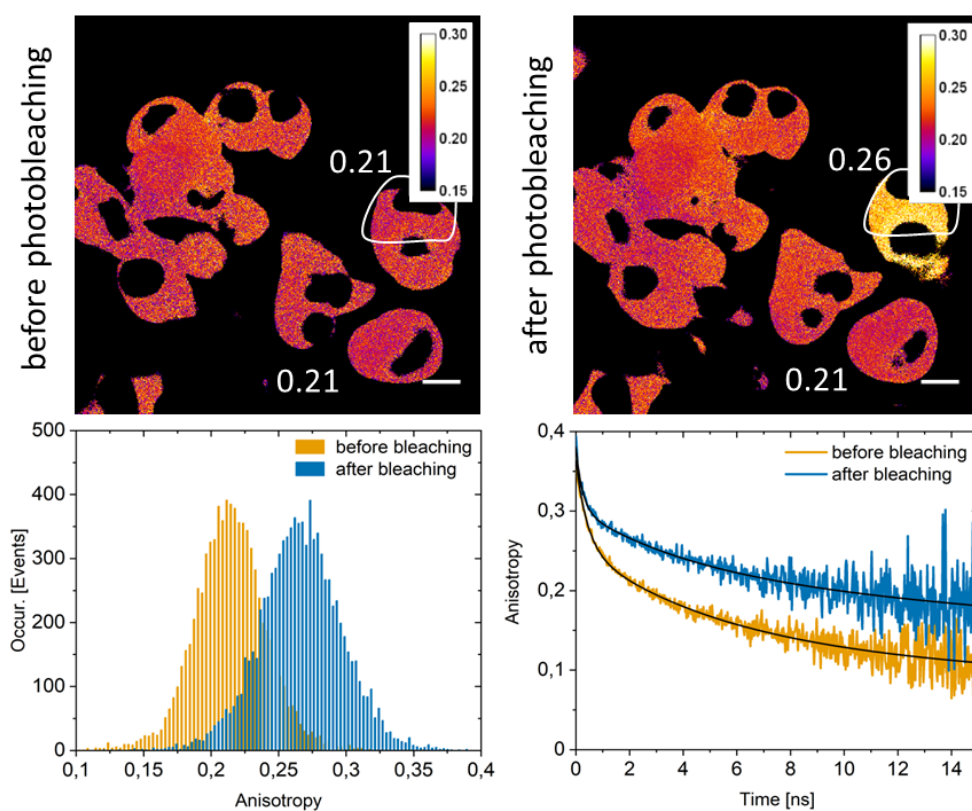


Figure 4.15: mVenus-tagged NPMmut homoFRET measurement.

4.3.2 NPMmut and p53mut

Further experiments were performed to investigate the interaction between NPMmut and p53mut proteins. NPMmut was tagged with mVenus fluorescent protein while p53mut was with mRFP1 fluorescent protein. In Fig.4.16 is shown an example of observing such labeled proteins in living cells.

The figure contains a record of two measurements (one row represents one measurement). The first column of the figure shows an intensity image for the mVenus protein indicating the localization of NPMmut; the second column contains intensity images of the mRFP protein, indicating the localization of p53mut; and the third column contains transmission images from an optical microscope. We can see NPMmut is mainly localized in cell cytoplasm while p53mut is localized solely in the nucleus, which is a distinct difference between the interaction of NPMmut with p53wt and p53mut. It indicates that p53mut is not able to bind to NPMmut protein.

The same results were obtained when using another combination of fluorescent labels, namely cyan fluorescent protein - Cerulean for p53mut and mVenus fluorescence protein for NPMmut. It goes without saying that heteroFRET experiments could not be conducted as the proteins of interest were physically in different locations.

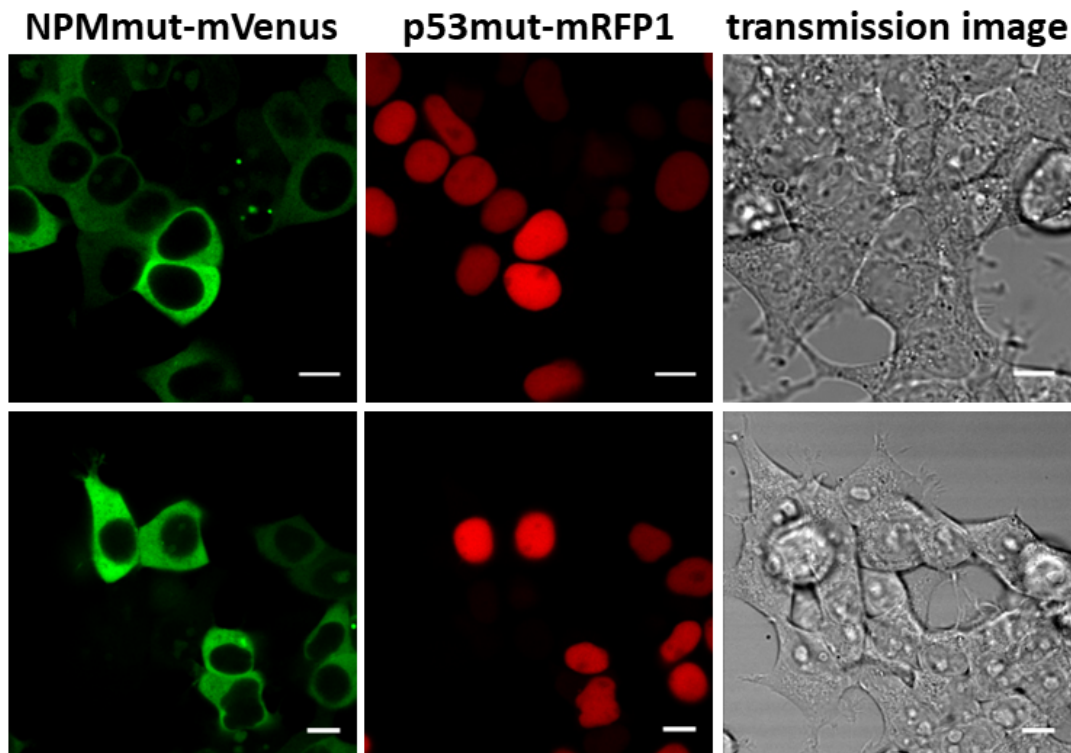


Figure 4.16: NPMmut_V and p53mut_R localization measurement. NPMmut was tagged with mVenus, while p53mut was tagged with mRFP1 fluorescent protein. One row shows the intensity image of mVenus, the intensity image of mRFP1 protein, and the transmission image, respectively. Two rows represent two different measurements of the same sample. The scale bar in all images represents 10 μm .

4.3.3 NPMmutcut and p53

Altogether with p53-NPMmut experiments p53-NPMmutcut experiments were performed. Since NPMmutcut can not form a homooligomer but still is localized in the cytoplasm with a p53wt, these experiments aim to determine whether p53wt homoFRET in the cytoplasm is observed due to the p53wt oligomeric state or p53wt monomer proximity in the NPMmut-p53wt complex.

4.3.4 NPMmutcut and p53wt

HeteroFRET experiments studying NPMmutcut-p53wt interaction in the cell cytoplasm were performed together with homoFRET experiments studying the p53wt oligomeric state in the NPMmutcut presence in the cell cytoplasm.

The results of the heteroFRET measurement are shown in Fig.4.17. From intensity images, we can see p53wt be pulled out from the cell nucleus to the cytoplasm as in the case of p53wt-NPMmut observation. Cells were bleached by 561 nm laser to zero mRFP1 intensity, and lifetime changes have been studied.

The measurement shown in Fig.4.17 shows the most significant lifetime change from all the performed measurements with these proteins, which is $\Delta\tau = 0.04$ ns. This change is similar to lifetime changes for the p53mut heteroFRET experiments and might show that p53wt is bound to NPMmutcut very weakly after being pulled out to the cytoplasm.

HomoFRET experiments were performed for p53wt labeled with the mVenus, and anisotropy changes were measured in the cell cytoplasm. Experiment results are shown in Fig.4.18. Steady-state anisotropy values averaged over a bleached cell are $r = 0.23$ before and $r = 0.26$ after photobleaching, resulting in anisotropy difference $\Delta r = 0.03$.

Anisotropy decay analysis was performed further. Anisotropy decay curves showed the best fit for a tri exponential decay model where ϕ_2 was chosen to be constant according to 3.4.2 and the absolute term was set to zero. The amplitude of the slow decaying component before bleaching was $A_2 = 0.12 \pm 0.01$; after bleaching, $A_2 = 0.18 \pm 0.01$. The amplitudes of the remaining two faster components had lower values in the state after bleaching; A_1 decreased from 0.05 ± 0.02 to 0.02 ± 0.02 , and A_3 decreased from 0.17 ± 0.02 to 0.13 ± 0.02 . A^* from A_1 and A_3 gives $A^* = 0.22 \pm 0.03$ before and $A^* = 0.15 \pm 0.03$ after photobleaching. The decrease in the combined amplitude of the fast components is compensated by the increase in the amplitude of the slow component indicating the presence of an energy transfer. Since NPMmutcut itself can not form an oligomer, we suggest that p53wt exists as an oligomer in the NPMmut-p53wt complex.

4.3.5 NPMmutcut and p53mut

In Fig.4.19, we can see the localization of the NPMmutcut (red) and p53mut (green) within the cell. NPMmutcut can be found in the cytoplasm and cell nucleus while p53mut is localized only in the cell nucleus as in the case of the NPMmut-p53mut observation.

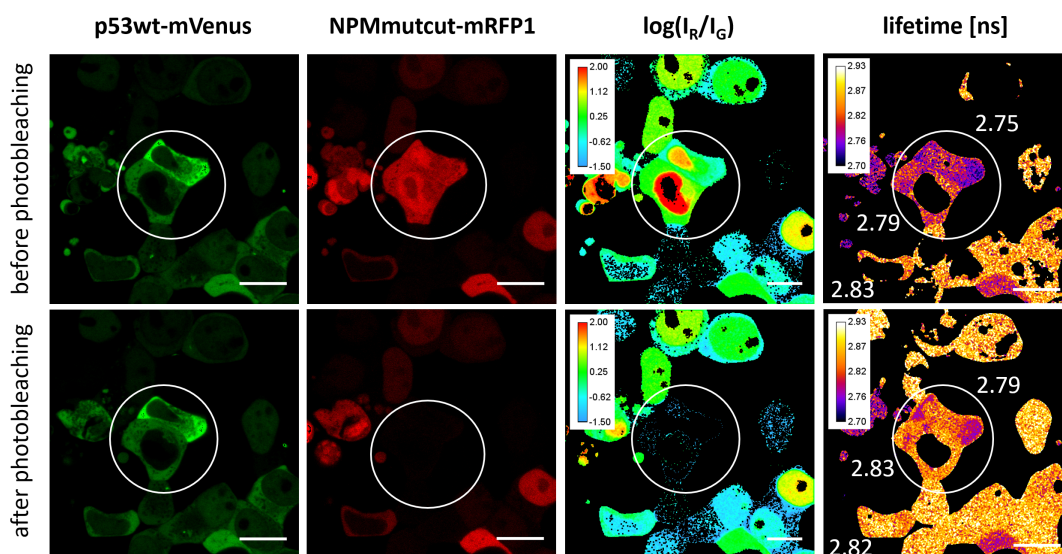


Figure 4.17: p53wt-NPMmutcut heteroFRET measurement. HEK-293T cells containing p53wt tagged with mVenus and NPMmutcut tagged with mRFP1 fluorescent protein.

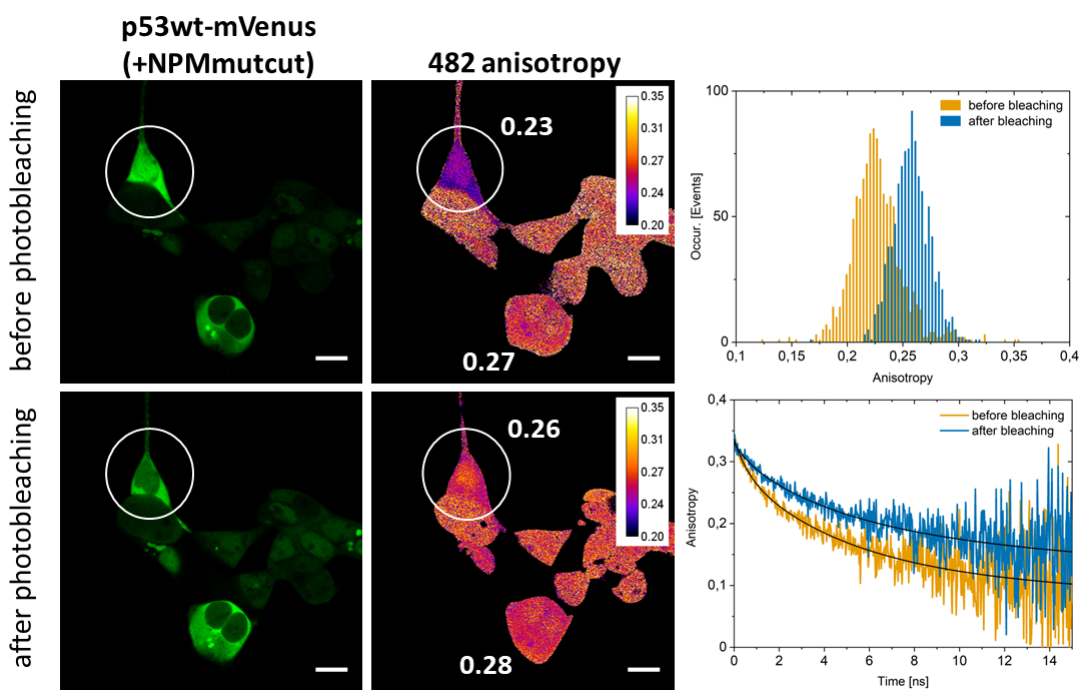


Figure 4.18: mVenus-tagged p53wt homoFRET measurement in the presence of NPMmutcut protein performed in a cell cytoplasm.

p53mut-mVenus **NPMmutcut-mRFP1** **transmission image**

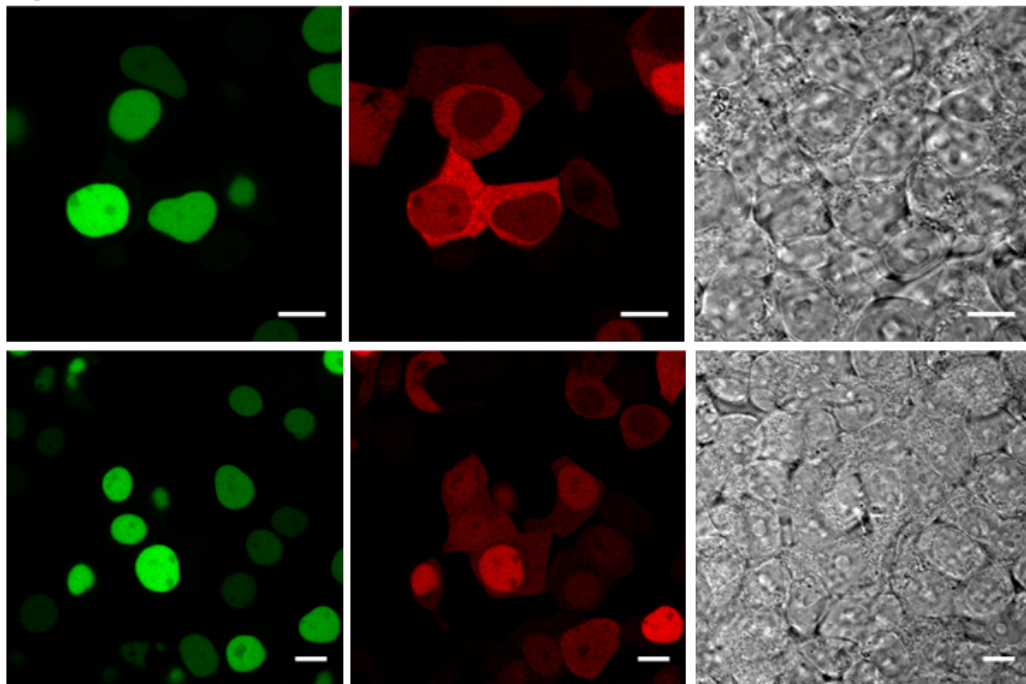


Figure 4.19: p53mut_V and NPMmutcut_R localization measurement. p53mut was tagged with mVenus, while NPMmutcut was tagged with mRFP1 fluorescent protein. One row shows the intensity image of mVenus, the intensity image of mRFP1 protein, and the transmission image, respectively. Two rows represent two different measurements of the same sample. The scale bar in all images represents 10 μm .

5. Discussion

In this chapter, I discuss the obtained results and the limitations of our approach and propose follow-up experiments.

5.1 Discussion of the results

p53wt heteroFRET and homoFRET experiments showed the most significant lifetime and anisotropy changes of all performed experiments, confirming the p53wt homooligomeric state in the cell nucleus as suggested by literature [14]. In the presence of NPMmut, p53wt protein was pulled out to the cytoplasm as observed in [13], indicating their interaction. The interaction has been confirmed by heteroFRET measurements when p53wt was labeled with mRFP1 while NPMmut was labeled with mVenus.

In the presence of NPMmutcut protein, p53wt was pulled from the nucleus into the cytoplasm indicating the p53wt-NPMmutcut complex formation. HeteroFRET measurement of the mVenus-tagged p53wt and the mRFP1-tagged NPMmutcut showed a similar lifetime change after photobleaching than the same proteins with reverse labeling studied in [13]. However, this lifetime change is at the significance limit. One possible reason for observing a more significant change in the donor's lifetime for the p53wt-NPMmut pair compared to the p53wt-NPMmutcut pair might be related to the different donor-to-acceptor ratio in the cytoplasm, where the heteroFRET measurements were conducted. In the case of p53wt-NPMmut, both proteins were observed almost exclusively in the cell cytoplasm. However, for the p53wt-NPMmutcut pair, while the p53wt was primarily localized in the cell cytoplasm, NPMmutcut showed bi-localization (nucleus and cytoplasm) with higher concentration in the nucleus. As NPMmutcut was labeled by a FRET acceptor (the mRFP1), the donor-to-acceptor ratio was smaller for p53wt-NPMmutcut pair compared to the p53wt-NPMmut pair.

However, according to the findings of the study [13], there is evidence to suggest a weaker interaction (lower binding affinity) between p53 and NPMmutcut compared to p53 and NPMmut. This conclusion is based on the lower amount of endogenous p53 that co-immunoprecipitated with NPMmutcut compared to NPMmut. Therefore, binding conditions in live cells might be unfavorable for detecting the complex by FRET.

When in a cytoplasm, mVenus-tagged p53wt protein appears to be in an oligomeric state, even if the detected homoFRET is weaker than in the nucleus. It needs to be clarified whether the oligomeric state is maintained during the transport by NPMmut or if the oligomers are only formed when in the cytoplasm.

As described in Section 4.1.2, the mVenus-tagged L344P mutant of p53 appeared to exhibit some degree of oligomer formation when observed *in vivo* contradicting the existing literature [14]. This discrepancy could be attributed to the nature of fluorescence microscopy, which involves the expression of proteins in cells through plasmid transfection. This artificial expression method often leads to protein overexpression compared to the naturally regulated levels of endogenous proteins within the cell. The continuous establishment of a balance between monomers and complexes within living cells suggests that complex formation may

occur as protein concentration increases, corresponding to an increase in the equilibrium constant. This assumption is supported by the observation that a change in anisotropy was detected in bright cells, even in the case of NPMcut, which should not be able to form oligomers.

The dependence of anisotropy on the fluorescent protein concentration is shown in Fig.5.1 where we can see pixel-by-pixel anisotropy to intensity graph of the selected areas (cells) marked by capital letters in corresponding intensity and anisotropy images. Data points representing intensity and anisotropy images' pixel values are fitted by a linear curve to highlight the decreasing character of this dependence. The decreasing character is observable only from a certain point, as the dispersion of values is too high for small intensities. For high signals, saturation is assumed.

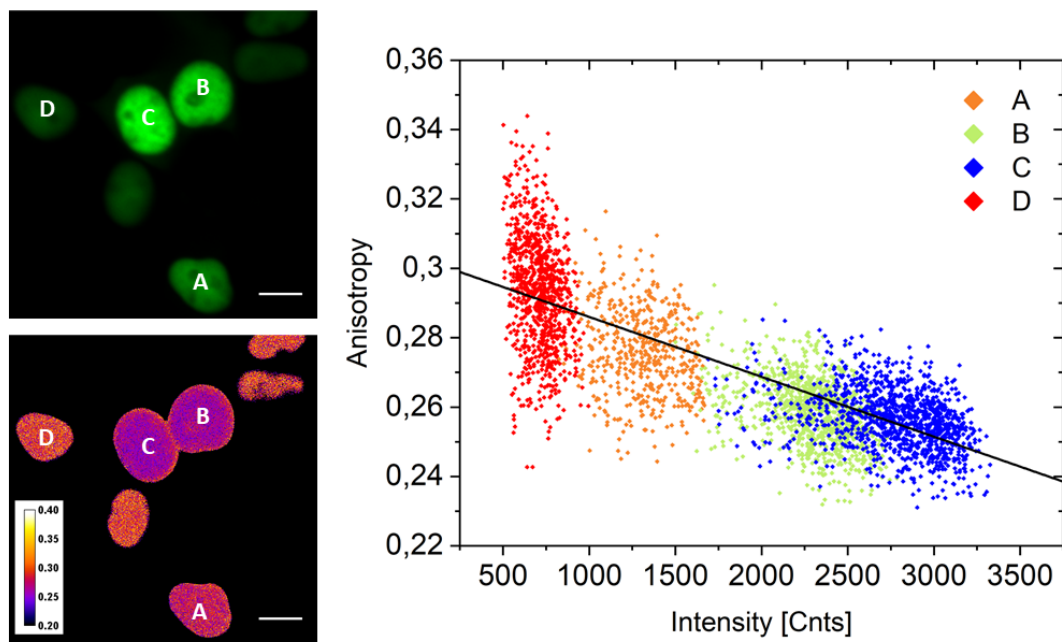
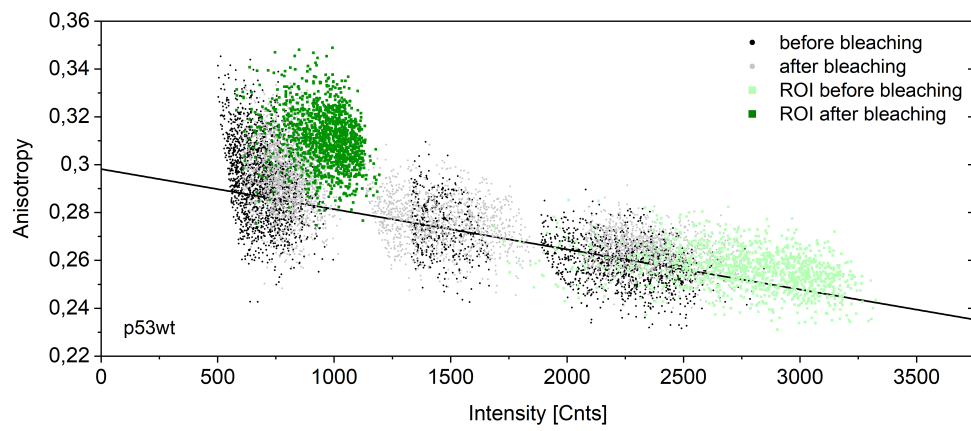
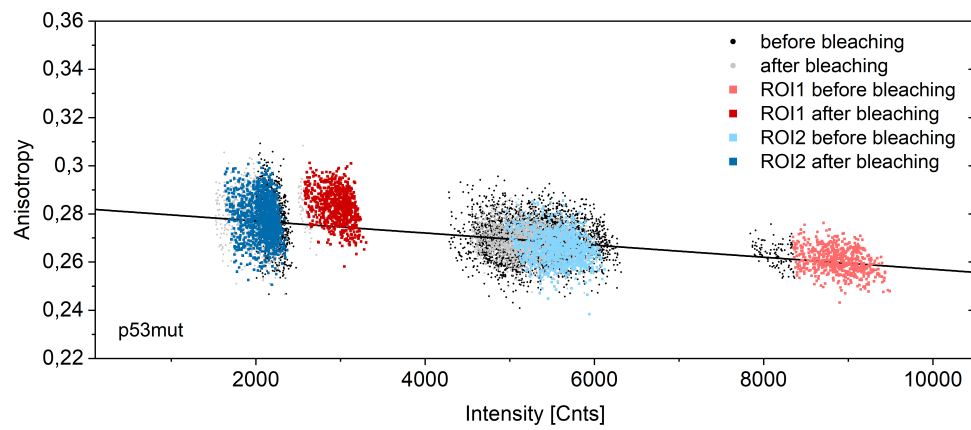


Figure 5.1: Pixel-by-pixel anisotropy to intensity image of chosen cells containing p53wt labeled by mVenus fluorescent protein. The figure shows decreasing dependence of anisotropy with cell intensity (fluorescent protein concentration).

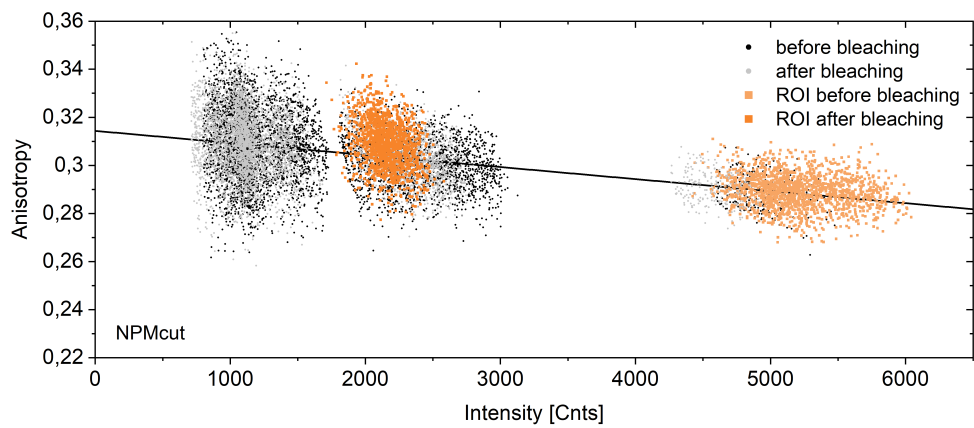
The comparison of the dependence of anisotropy on cell intensity between p53wt and p53mut is shown in Fig.5.2a and Fig.5.2b, respectively. The dependence is more clearly visible for p53wt, a complex-forming protein, than for p53mut. The graph plotted in this way might help in indicating a difference between interacting and non-interacting complexes; after bleaching cells containing p53mut or NPMcut, corresponding data points in the graph shift to a higher anisotropy but follow the curve trend and remain in the variance around it (see Fig.5.2b, Fig.5.2c). However, after bleaching the cells containing oligomerizing complex, data points move outside the band, defined by the points before bleaching (see Fig.5.2a). This observation currently remains a hypothesis that requires further confirmation through additional measurements. The problem with this method is covering a sufficient range of cells' intensities in one field, which is often challenging to achieve.



(a)



(b)



(c)

Figure 5.2: Pixel-by-pixel intensity-to-anisotropy graphs for (a) p53wt, (b) p53mut and (c) NPMcut labeled by mVenus.

Taking into account the concentration-dependent equilibrium shifts, our data suggest that the multimerization capacity of p53mut is much weaker than that of p53wt. We, therefore, conclude that at physiologically low concentrations p53mut is likely monomeric, as suggested in the literature [14].

Since NPMmut interaction with p53wt proved to cause a displacement from its mainly nuclear localization to the cytoplasm, thus perturbing its function in apoptosis and cell cycle regulation, it is important to study its transport back to the cytoplasm.

To our knowledge, the interaction of the monomeric p53-L344P with p53wt or NPMmut has not been studied *in vivo* yet, and the results presented in the thesis are, therefore, novel to this date.

Disjunct localization of the p53mut and NPMmut in HEK-293T cells suggest that these proteins do not interact. However, the reason why p53mut is not being pulled to the cytoplasm remains unanswered. We suggest that it might be related to the p53mut monomeric state as opposed to the p53wt oligomer. The p53mut and NPMwt mutual interaction in the cell nucleus should be investigated to complement this study.

The other reason for preventing p53mut from leaving the nucleus might be that the L344P mutation is present in the nuclear export signal (NES) sequence (340-351 p53 residue [24]). Therefore, another monomeric form of the p53 protein with the mutation outside the NES region should be studied.

According to [52], NPM interacts with two regions of p53 - residues 175-196 and residues 343-363. The second region contains the location of the L344P point mutation, so the reason why p53mut is not transported to the cytoplasm might be the perturbed interaction site.

As an additional remark in this discussion, I would like to mention that although the use of the faulty mVenus tagged-p53mut construct (which was the focus of our research alongside p53wt) set us back for a while, it did provide valuable insights through the eloquence of the experimental data. The measurements conducted with the faulty construct yielded results that contradicted the assumed theory, ultimately leading us to discover the error. It is always prudent to formulate hypotheses about the expected outcome of an experiment and not consider the results definitive until they have been verified by a series of measurements using other independent experimental methods.

5.2 Asymmetry of reverse fluorescent labeling

The results of several experiments turned out to be different when different fluorescent labeling was used - these are measurements of the mutual interaction of p53wt and p53mut in the nucleus and the interaction of p53wt with NPMmut in the cytoplasm. Similar results have been observed in [48] when studying NPMmut and NPMmutcut interaction. Asymmetry might be caused by different fluorescent label orientations when attached to studied proteins which cause different FRET efficiency. Although fluorescent labels are unlikely to influence the 'natural' oligomerization properties of the studied proteins, some labeling might modulate complex formation.

Different results were also obtained with different fluorescent labels for anisotropy measurement. mRFP1 homoFRET experiments did not confirm the mVe-

nus homoFRET results for the p53wt protein. This inconsistency can be caused, i. g., by a smaller Förster radius of the mRFP1 pair ($R_0 = 44.65 \text{ \AA}$) compared to the mVenus pair ($R_0 = 51.97 \text{ \AA}$) or again by different mutual fluorescent protein orientations when attached to p53wt resulting in the lowered efficiency of the energy transport.

All these observations primarily highlight the importance of working with multiple fluorescent labels and comparing the results among them.

5.3 Time-resolved anisotropy analysis

To obtain anisotropy curves, one must follow a multi-step process. Each step might introduce an error to the final anisotropy values. In some of the obtained anisotropy decays in this thesis, anisotropy decays before and after photobleaching do not have a common origin, although it contradicts the theory. This might be caused by incorrect background subtraction from the polarized intensity curves, incorrect determination of the time origin of the decay, or incorrect determination of the G-factor. The noise in the intensity decay data causes an immense contribution to the error, since the data acquisition time is limited as the cells might move or undergo degenerative processes. Improving the signal-to-noise ratio could be achieved by searching for a photostable protein with a larger quantum yield or by enhancing the photon collection efficiency of the experimental setup. Another source of error is likely the use of a simplified model for anisotropy decay, which is derived for globular proteins [4]. The proteins being studied may have asymmetrical shapes and consist of more complex decay components, making the simplified model inappropriate.

In conclusion, due to the significant uncertainties in the parameters, the anisotropy decay analysis is a qualitative rather than a quantitative method at this stage.

Conclusion

In this work, we used the newly introduced anisotropy imaging method together with the lifetime imaging method to study the L344P mutant of tumor suppressor p53 - p53mut, and its interaction with p53wt, NPMmut, and NPMmutcut (for NPM mutations used in this thesis see Fig.1.4). For comparison, we supplemented the experiments with those of already investigated p53wt and p53wt-NPMmut(cut) complexes.

HeteroFRET experiments performed on p53mut labeled respectively by mVenus and mRFP1, and homoFRET experiments performed on p53mut labeled by mVenus indicate a weak interaction of this protein at high concentrations. However, it is very likely that at the physiological concentrations in the cell, p53mut assembles in a monomeric state, as suggested by existing literature.

Using heteroFRET experiments, we further showed the probable formation of complexes between p53wt and p53mut. A more pronounced change in lifetime was observed when labeling p53wt with mVenus and p53mut with mRFP1, compared to the opposite labeling scheme of p53wt with mRFP1 and p53mut with mVenus. The discussion briefly addresses the asymmetry observed in the experimental results when using different labeling combinations for the investigated proteins.

While in NPMmut experiments with p53wt, the p53 protein was pulled into the cytoplasm, experiments with p53mut showed disjunctive localization for NPMmut and p53mut, with NPM located in the cytoplasm and p53mut in the nucleus.

The interaction between NPMmut-mVenus and p53wt-mRFP1 in the cytoplasm was confirmed by heteroFRET experiments. Separately performed homoFRET experiments indicated the oligomeric state of p53wt and NPMmut proteins in the cytoplasm.

When co-expressed with the monomeric NPMmutcut - localized in the nucleus and cell cytoplasm, p53wt was found in the cytoplasm, while p53mut was present exclusively in the nucleus. These were two different experiments where only one of the p53 proteins was co-expressed with NPMmutcut. A co-localization experiment with triple labeling that would simultaneously monitor co-expressed p53wt, p53mut, and NPMmut(cut) is left for further study. Although the interaction of p53wt with NPMmutcut seems to be weak in heteroFRET measurements, a combination of homoFRET and co-localization experiments indicate the existence of transient p53wt-NPMmutcut complex in cytoplasm, with p53wt being in the oligomeric state.

Additionally, anisotropy measurements in the red spectral range using the mRFP1 fluorescent protein were conducted. However, this fluorescent label has proved to be unsuitable for homoFRET experiments on p53mut and p53wt samples since, in neither case did it show a significant shift in anisotropy (see Fig.4.7 and Fig.4.8).

To summarize, this study demonstrates that p53mut likely exists as a monomeric form and can form complexes with p53wt. However, it does not engage in complex formation with NPMmut or NPMmutcut. While several plausible explanations for this observation have been considered, a definitive answer awaits further investigation.

Bibliography

- [1] B. Valeur and M. N. Berberan-Santos. A brief history of fluorescence and phosphorescence before the emergence of quantum theory. *Journal of Chemical Education*, 88(6):731–738, Jun 2011.
- [2] H. Virk. History of luminescence from ancient to modern times. *Defect and Diffusion Forum*, Vol. 361 (2015) pp 1-13:1–13, 01 2015.
- [3] C. A. Combs. Fluorescence microscopy: a concise guide to current imaging methods. *Curr Protoc Neurosci*, Chapter 2:Unit2.1, January 2010.
- [4] J. R. Lakowicz. *Principles of Fluorescence Spectroscopy*. Springer Science Business Media, LLC, New York, 2006.
- [5] S. W. Hell and J. Wichmann. Breaking the diffraction resolution limit by stimulated emission: stimulated-emission-depletion fluorescence microscopy. *Opt Lett*, 19(11):780–782, June 1994.
- [6] J. K. Sanders and S. E Jackson. The discovery and development of the green fluorescent protein, GFP. *Chem Soc Rev*, 38(10):2821–2822, September 2009.
- [7] G. U. Nienhaus. The green fluorescent protein: a key tool to study chemical processes in living cells. *Angew Chem Int Ed Engl*, 47(47):8992–8994, 2008.
- [8] O. Griesbeck. Fluorescent proteins as sensors for cellular functions. *Current Opinion in Neurobiology*, 14(5):636–641, 2004.
- [9] M. Yang, P. Jiang, N. Yamamoto, et al. Real-time whole-body imaging of an orthotopic metastatic prostate cancer model expressing red fluorescent protein. *Prostate*, 62(4):374–379, March 2005.
- [10] D. A. Zacharias, J. D. Violin, A. C. Newton, and R. Y. Tsien. Partitioning of lipid-modified monomeric gfps into membrane microdomains of live cells. *Science*, 296(5569):913–916, 2002.
- [11] D. S. Goodsell and A. J. Olson. Structural symmetry and protein function. *Annu Rev Biophys Biomol Struct*, 29:105–153, 2000.
- [12] F. Shekari, H. Baharvand, and G. H. Salekdeh. Chapter seven - organellar proteomics of embryonic stem cells. In Rossen Donev, editor, *Proteomics in Biomedicine and Pharmacology*, volume 95 of *Advances in Protein Chemistry and Structural Biology*, pages 215–230. Academic Press, 2014.
- [13] A. Holoubek, D. Strachotová, P. Otevřelová, et al. AML-related NPM mutations drive p53 delocalization into the cytoplasm with possible impact on p53-dependent stress response. *Cancers*, 13(13), 2021.
- [14] G. Gaglia, Y. Guan, J. V. Shah, and G. Lahav. Activation and control of p53 tetramerization in individual living cells. *Proc Natl Acad Sci U S A*, 110(38):15497–15501, September 2013.

- [15] N. W. Fischer, A. Prodeus, J. Tran, et al. Association between the oligomeric status of p53 and clinical outcomes in Li-Fraumeni syndrome. *J Natl Cancer Inst*, 110(12):1418–1421, December 2018.
- [16] F. P. Li and J. F. Fraumeni, Jr. Soft-tissue sarcomas, breast cancer, and other neoplasms. a familial syndrome? *Ann Intern Med*, 71(4):747–752, October 1969.
- [17] M. Olivier, M. Hollstein, and P. Hainaut. TP53 mutations in human cancers: origins, consequences, and clinical use. *Cold Spring Harb Perspect Biol*, 2(1):a001008, January 2010.
- [18] Medlineplus, National Library of Medicine (US): TP53 gene. <https://medlineplus.gov/genetics/gene/tp53/>. Accessed: 2023-03-15.
- [19] F. Perri, S. Pisconti, and G. Della Vittoria Scarpati. P53 mutations and cancer: a tight linkage. *Ann Transl Med*, 4(24):522, December 2016.
- [20] Y. Liu, O. Tavana, and W. Gu. p53 modifications: exquisite decorations of the powerful guardian. *J Mol Cell Biol*, 11(7):564–577, July 2019.
- [21] R. A. Gjerset. Dna damage, p14ARF, nucleophosmin (NPM/B23), and cancer. *Journal of Molecular Histology*, 37(5):239–251, Sep 2006.
- [22] S. Kurki, K. Peltonen, L. Latonen, et al. Nucleolar protein NPM interacts with HDM2 and protects tumor suppressor protein p53 from HDM2-mediated degradation. *Cancer Cell*, 5(5):465–475, May 2004.
- [23] E. Schneider, M. Montenarh, and P. Wagner. Regulation of CAK kinase activity by p53. *Oncogene*, 17(21):2733–2741, Nov 1998.
- [24] J. Gencel-Augusto and G. Lozano. p53 tetramerization: at the center of the dominant-negative effect of mutant p53. *Genes Dev*, 34(17-18):1128–1146, September 2020.
- [25] K. G. McLure and P. W. Lee. How p53 binds DNA as a tetramer. *EMBO J*, 17(12):3342–3350, June 1998.
- [26] R. L. Weinberg, D. B. Veprintsev, and A. R. Fersht. Cooperative binding of tetrameric p53 to DNA. *J Mol Biol*, 341(5):1145–1159, August 2004.
- [27] Y. Itahana, H. Ke, and Y. Zhang. p53 oligomerization is essential for its c-terminal lysine acetylation. *J Biol Chem*, 284(8):5158–5164, December 2008.
- [28] P. R. Mittl, P. Chène, and M. G. Grütter. Crystallization and structure solution of p53 (residues 326-356) by molecular replacement using an NMR model as template. *Acta Crystallogr D Biol Crystallogr*, 54(Pt 1):86–89, January 1998.
- [29] H. Tidow, R. Melero, E. Mylonas, et al. Quaternary structures of tumor suppressor p53 and a specific p53 DNA complex. *Proc Natl Acad Sci U S A*, 104(30):12324–12329, July 2007.

- [30] E. Colombo, M. Alcalay, and P. G. Pelicci. Nucleophosmin and its complex network: a possible therapeutic target in hematological diseases. *Oncogene*, 30(23):2595–2609, January 2011.
- [31] L. Federici and B. Falini. Nucleophosmin mutations in acute myeloid leukemia: a tale of protein unfolding and mislocalization. *Protein Sci*, 22(5):545–556, March 2013.
- [32] D. A. Maignel, L. Jones, D. Chakravarty, et al. Nucleophosmin sets a threshold for p53 response to UV radiation. *Mol Cell Biol*, 24(9):3703–3711, May 2004.
- [33] J. Li, X. Zhang, D. P. Sejas, and Q Pang. Negative regulation of p53 by nucleophosmin antagonizes stress-induced apoptosis in human normal and malignant hematopoietic cells. *Leukemia Research*, 29(12):1415–1423, 2005.
- [34] S. K. Dhar and D. K. St Clair. Nucleophosmin blocks mitochondrial localization of p53 and apoptosis. *J Biol Chem*, 284(24):16409–16418, April 2009.
- [35] B. Falini, C. Mecucci, E. Tiacci, et al. Cytoplasmic nucleophosmin in acute myelogenous leukemia with a normal karyotype. *N Engl J Med*, 352(3):254–266, January 2005.
- [36] B. Falini, N. Bolli, J. Shan, et al. Both carboxy-terminus NES motif and mutated tryptophan(s) are crucial for aberrant nuclear export of nucleophosmin leukemic mutants in NPMc+ AML. *Blood*, 107(11):4514–4523, 06 2006.
- [37] J. A. Levitt, D. R. Matthews, S. M. Ameer-Beg, and K. Suhling. Fluorescence lifetime and polarization-resolved imaging in cell biology. *Curr Opin Biotechnol*, 20(1):28–36, March 2009.
- [38] Jing Z. and Shirui M. Chapter three - tuning the membrane fluidity of liposomes for desirable in vivo fate with enhanced drug delivery. volume 34 of *Advances in Biomembranes and Lipid Self-Assembly*, pages 67–106. Academic Press, 2021.
- [39] M. K. Kuimova. Mapping viscosity in cells using molecular rotors. *Phys. Chem. Chem. Phys.*, 14:12671–12686, 2012.
- [40] A. Boza-Serrano, R. Ruiz, R. Sanchez-Varo, et al. Galectin-3, a novel endogenous TREM2 ligand, detrimentally regulates inflammatory response in alzheimer’s disease. *Acta Neuropathologica*, 138(2):251–273, Aug 2019.
- [41] A. Gijsbers, T. Nishigaki, and N. Sánchez-Puig. Fluorescence anisotropy as a tool to study protein-protein interactions. *J Vis Exp*, (116), October 2016.
- [42] S. Vogel, C. Thaler, Blank P., and Koushik S. *FLIM Microscopy in Biology and Medicine*, chapter 10, Time-Resolved Fluorescence Anisotropy, pages 245–290. 1st edition. Chapman and Hall/CRC, New York, 2009.

- [43] O. Shimomura, F. H. Johnson, and Y. Saiga. Extraction, purification and properties of aequorin, a bioluminescent protein from the luminous hydromedusa, *aequorea*. *J Cell Comp Physiol*, 59:223–239, June 1962.
- [44] T. J. Lambert. FPbase: a community-editable fluorescent protein database. *Nature Methods*, 16(4):277–278, Apr 2019.
- [45] T. Lambert. The fluorescent protein database. <https://www.fpbases.org/>. Accessed: 2023-03-07.
- [46] A. Vacková. *en. MA thesis Properties and interactions of nucleoproteins studied by advanced lifetime-based imaging methods*. Institute of Physics of Charles University, MFF, Charles University, Prague, 2022.
- [47] B. Brodská, A. Holoubek, P. Otevřelová, and K. Kuželová. Low-Dose Actinomycin-D induces redistribution of Wild-Type and mutated nucleophosmin followed by cell death in leukemic cells. *J Cell Biochem*, 117(6):1319–1329, November 2015.
- [48] M. Šašínková, P. Heřman, A. Holoubek, D. Strachotová, et al. Nsc348884 cytotoxicity is not mediated by inhibition of nucleophosmin oligomerization. *Scientific Reports*, 11(1):1084, Jan 2021.
- [49] V. Devauges, C. Marquer, S. Lecart, et al. Homodimerization of amyloid precursor protein at the plasma membrane: A homofret study by time-resolved fluorescence anisotropy imaging. *PloS one*, 7:e44434, sep 2012.
- [50] S. T. Hess, E. D. Sheets, et al. Quantitative analysis of the fluorescence properties of intrinsically fluorescent proteins in living cells. *Biophys J*, 85(4):2566–2580, October 2003.
- [51] M. Kitayner, H. Rozenberg, N. Kessler, et al. Structural basis of DNA recognition by p53 tetramers. *Mol Cell*, 22(6):741–753, June 2006.
- [52] B. Lambert and M. Buckle. Characterisation of the interface between nucleophosmin (NPM) and p53: potential role in p53 stabilisation. *FEBS Lett*, 580(1):345–350, December 2005.

List of Figures

1.1	p53 domain structure.	5
1.2	Tetramerization domain of the p53 wt protein.	6
1.3	flp53 and its tetramerization domain structure.	7
1.4	NPM structure and mutation overview.	7
2.1	Simplified Jablonski diagram.	10
2.2	FLIM image with corresponding decay curve.	12
2.3	The emission and excitation spectra of mVenus and mRFP1 heteroFRET fluorescent protein pair.	14
3.1	Scheme of stepwise preparation of plasmids including p53mut molecular cloning.	16
3.2	The simplified ray path scheme in confocal lifetime and anisotropy measurements.	17
3.3	G-factor determining procedure.	18
4.1	p53wt heteroFRET measurement.	23
4.2	mVenus-tagged p53wt homoFRET measurement.	24
4.3	p53mut heteroFRET measurement.	25
4.4	p53 heteroFRET pairwise comparison.	25
4.5	mVenus-tagged p53mut homoFRET measurement.	26
4.6	p53 homoFRET pairwise comparison.	27
4.7	p53wt_mRFP1 homoFRET experiment.	28
4.8	p53mut_mRFP1 homoFRET experiment.	29
4.9	p53mut_V-p53wt_R heteroFRET measurement.	29
4.10	p53wt_V-p53mut_R heteroFRET measurement.	30
4.11	mVenus-tagged NPMcut homoFRET measurement.	31
4.12	p53wt_V-NPMmut_R heteroFRET measurement.	32
4.13	mVenus-tagged p53wt homoFRET measurement in the presence of NPMmut.	32
4.14	NPMmut_V-p53wt_R heteroFRET measurement.	34
4.15	mVenus-tagged NPMmut homoFRET measurement.	34
4.16	NPMmut_V and p53mut_R localization measurement.	35
4.17	p53wt_V-NPMmutcut_R heteroFRET measurement.	37
4.18	mVenus-tagged p53wt homoFRET measurement in the presence of NPMmutcut.	37
4.19	p53mut_V and NPMmutcut_R localization measurement.	38
5.1	p53mut_V Pixel-by-pixel anisotropy to intensity image of chosen cells.	40
5.2	Pixel-by-pixel intensity-to-anisotropy graphs for p53wt, p53mut, and NPMcut labeled by mVenus.	41

List of Tables

A.1	Bi-exponential fit for mVenus-tagged p53wt anisotropy decay before (A) and after bleaching (B)	51
A.2	Bi-exponential fit for mVenus-tagged p53mut anisotropy decay before (A) and after bleaching (B)	51
A.3	Bi-exponential fit for mVenus-tagged NPMcut anisotropy decay before (A) and after bleaching (B)	51
A.4	Bi-exponential fit for mVenus-tagged p53wt anisotropy decay in cell cytoplasm after being pulled out by NPMmut before (A) and after bleaching (B)	51
A.5	Tri-exponential fit for mVenus-tagged NPMmut anisotropy decay before (A) and after bleaching (B)	51
A.6	Tri-exponential fit for mVenus-tagged p53wt anisotropy decay in cell cytoplasm after being pulled out by NPMmutcut before (A) and after bleaching (B)	51

A. Review of anisotropy decay fitting

Table A.1: Bi-exponential fit for mVenus-tagged p53wt anisotropy decay before (A) and after bleaching (B)

	A_1	ϕ_1	A_2	ϕ_2	r_∞
A	0.20 ± 0.01	4.4 ± 0.2	0.15 ± 0.01	36	0
B	0.07 ± 0.01	4.0 ± 0.5	0.29 ± 0.01	36	0

Table A.2: Bi-exponential fit for mVenus-tagged p53mut anisotropy decay before (A) and after bleaching (B)

	A_1	ϕ_1	A_2	ϕ_2	r_∞
A	0.11 ± 0.02	5.1 ± 0.9	0.19 ± 0.04	36	0.01 ± 0.02
B	0.05 ± 0.01	5.1 ± 0.9	0.26 ± 0.04	36	0.01 ± 0.02

Table A.3: Bi-exponential fit for mVenus-tagged NPMcut anisotropy decay before (A) and after bleaching (B)

	A_1	ϕ_1	A_2	ϕ_2	r_∞
A	0.23 ± 0.13	9 ± 2	0.00 ± 0.14	16	0.11 ± 0.01
B	0.07 ± 0.07	9 ± 2	0.17 ± 0.08	16	0.11 ± 0.01

Table A.4: Bi-exponential fit for mVenus-tagged p53wt anisotropy decay in cell cytoplasm after being pulled out by NPMmut before (A) and after bleaching (B)

	A_1	ϕ_1	A_2	ϕ_2	r_∞
A	0.15 ± 0.05	5.2 ± 1.6	0.20 ± 0.14	36	0
B	0.07 ± 0.04	4.4 ± 2.7	0.29 ± 0.11	36	0

Table A.5: Tri-exponential fit for mVenus-tagged NPMmut anisotropy decay before (A) and after bleaching (B)

	A_1	ϕ_1	A_2	ϕ_2
A	0.11 ± 0.01	0.36 ± 0.05	0.11 ± 0.12	77
B	0.07 ± 0.01	0.36 ± 0.05	0.20 ± 0.12	77
	A_3	ϕ_3	A	r_∞
A	0.14 ± 0.02	5.1 ± 1.3	0.25 ± 0.02	0
B	0.09 ± 0.02	5.1 ± 1.3	0.16 ± 0.02	0

Table A.6: Tri-exponential fit for mVenus-tagged p53wt anisotropy decay in cell cytoplasm after being pulled out by NPMmutcut before (A) and after bleaching (B)

	A_1	ϕ_1	A_2	ϕ_2
A	0.05 ± 0.02	0.61 ± 0.60	0.12 ± 0.01	36
B	0.02 ± 0.02	0.61 ± 0.60	0.18 ± 0.01	36
	A_3	ϕ_3	A	r_∞
A	0.17 ± 0.02	4.7 ± 1.2	0.22 ± 0.03	0
B	0.13 ± 0.02	4.7 ± 1.2	0.15 ± 0.03	0